Politecnico di Torino

Laurea Magistrale in Ingegneria dei Materiali per l'industria 4.0

A.A. 2024/2025

Sessione di Laurea Marzo 2025

Polimorfismo dell'orcinolo

Relatori:

Maria del Barrio Casado

Marco Sangermano

Candidato:

Stefano Krstov

Ringraziamenti

Vorrei ringraziare il Group of Characterisation of Materials (GCM) dell'Universitat Politecnica de Catalunya per avermi concesso la possibilità di svolgere questa tesi di ricerca presso i loro laboratori. Vorrei in particolare ringraziare la mia relatrice, Maria del Barrio, per avermi seguito durante il lavoro sperimentale e nella stesura. Ringrazio inoltre il professor Marco Sangermano che, in qualità di coordinatore delle attività di mobilità e di co-relatore, mi ha seguito e consigliato durante il periodo di svolgimento della tesi.

Ringrazio infine i colleghi e gli amici che sono stati presenti in questi anni, ma soprattutto ringrazio i miei genitori senza i cui sacrifici questo percorso non sarebbe stato possibile.

Sommario

Questo studio si concentra sul polimorfismo (capacità di un solido di esistere in molteplici forme cristalline) di un composto organico detto orcinolo. Lo scopo della ricerca è indagare la relazione termodinamica tra i diversi polimorfi in un intervallo di pressione fino a 300 MPa mediante tecniche calorimetriche (TGA, DSC, HP-DTA). Inoltre, sono state utilizzate misure di diffrazione ai raggi X (XRD) per cercare di identificare il reticolo cristallino di questi polimorfi.

L'analisi termica a pressione ambiente ha rivelato l'esistenza di tre distinti punti di fusione a 108,87 °C, 97,06 °C e 84,24 °C, corrispondenti alla fusione di tre fasi solide denominate I, II e III, rispettivamente. Un ragionamento condotto a partire da considerazioni termodinamiche ha portato a proporre una relazione monotropica tra I, II e III a pressione ambiente.
Misure complementari ai raggi X hanno permesso di identificare la fase I con la struttura tetragonale riportata in bibliografia. Come risultato dagli esperimenti di analisi termica, con il raffreddamento del campione dallo stato liquido si è ottenuta la cristallizzazione di diversi polimorfi. Purtroppo, i dati raccolti non consentono di compiere una precisa corrispondenza tra le celle cristalline determinate da XRD e le forme polimorfiche metastabili ottenute durante le analisi termiche.
L'analisi termica differenziale ad alta pressione (HP-DTA) è stata utilizzata per registrare l'evoluzione dei punti di fusione in funzione della pressione, creando un diagramma sperimentale pressione-temperatura.
La maggior pendenza della curva di equilibrio II-L rispetto a quella dell'equilibrio I-L suggerisce l’esistenza di un punto triplo a circa 270 MPa; a partire da questa pressione la relazione tra le fasi I e II diventa enantiotropica. Invece, le fasi II e III sono complessivamente correlate in modo monotropo.

Abstract

This study focuses on polymorphism, which is the ability of a solid to exist in multiple crystalline forms, of one organic compound called orcinol. The aim of the research is to investigate the thermodynamic relationship between the different polymorphous in a range of pressure up to 300 MPa by means of calorimetric techniques. Furthermore, X-ray diffraction measurements have been used to try to identify the crystal lattice of these polymorphs.

Thermal analysis at normal pressure has revealed the existence of three distinct melting points at 108,87 °C, 97,06 °C, and 84,24 °C, corresponding to the melting of three solid phases, I, II and III, respectively. By thermodynamic reasoning, a monotropic relation between them has been proposed at this pressure. Complementary X-ray measurements have allowed to identify phase I with the tetragonal structure reported in the bibliography. As in thermal analysis experiments, cooling the sample from the liquid state produced the crystallization of different polymorphs. Unfortunately, the data does not allow to identify the lattices corresponding to the metastable polymorphous obtained by thermal analysis.

High-pressure differential thermal analysis (HP-DTA) was used to record the evolution of the melting points as a function of the pressure, creating an experimental pressure-temperature diagram. The higher (experimental) value of the slope of the II-L equilibrium compared to that of the I-L equilibrium gives clue of the existence of a triple point around 270 MPa, then from this pressure the relation between phases I and II becomes enantiotropic. Instead, phases II and III are monotropically related overall.

Index

1. Thermodynamics overview

1.1 Thermodynamic system and thermodynamic variables

To define a thermodynamic system, one must isolate a specific portion of matter or substance that becomes the focus of study. This involves designating a closed surface that encloses a part of the universe, with the boundary being the system border, which separates the system from its surroundings. Additionally, it is important to manage the exchanges between the system and its environment. The system should contain many particles, meaning it cannot be too small.

Assuming a substance's atomic structure, it is understood that a complex organization of molecules is possible at the macro level. While a detailed microscopic description, involving individual particles interacting in a specific field, is conceivable, such precision is unnecessary for defining macroscopic principles. Moreover, a fully accurate microscopic depiction is theoretically possible but impractical. Thus, new variables that describe broad characteristics or large-scale properties of the system are introduced to provide a macroscopic view [1].

1.2 State equations and p-V-T diagrams

State equations are algebraic expressions that establish relationships between key state variables like pressure, volume, temperature, and the quantity of a pure substance or a mixture in a thermodynamic system. These equations are valuable for characterizing matter and determining the properties of liquid, solid, or gas and vapor phases under various conditions, depending on their thermodynamic applicability. Additionally, the thermal equation of state in a simple pVT system describes the system's equilibrium state, correlating non-energy thermodynamic variables such as pressure (p), temperature (T), density (ρ), and volume (V).
This equation is usually reformulated so that it depends solely on the substance(s), not on the amount or size of the substance(s) being measured. This is done by replacing extensive properties with their intensive values per unit of mass or mole. For example, combining the variables V and m results in v ($v = V/m$), an intensive property. The state equation [2], if the system comprises of a single pure substance, is:

$$f(p, T, v) = 0 \qquad \text{Eq. 1.1}$$

On the other hand, a phase diagram is a graphical tool that shows the values of thermodynamic variables when the system's phases are in equilibrium. These diagrams have been essential tools for materials science and development for many years. By representing equation Eq. 1.1 in a rectangular coordinate system with axes for p, v, and T, one can derive the so-called $p{-}v{-}T$ surface [3], as illustrated in Figure 1.1.

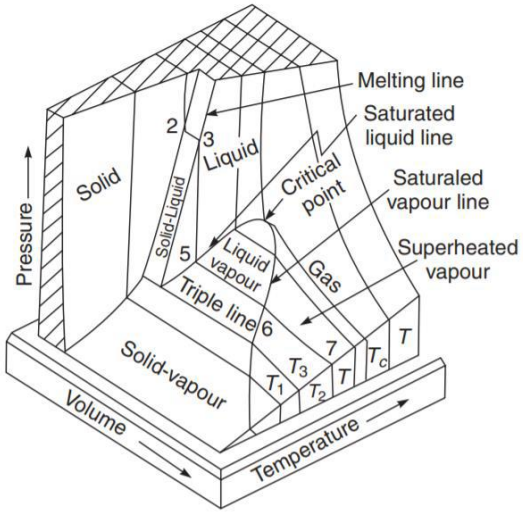

Figure 1.1. p−v−T diagram of a pure substance [4]

Additionally, by projecting these surfaces onto the p−T and p−v planes (Fig 1.2), the corresponding diagrams for p−T and p−v are obtained. The projection on the p−T diagram in Figure 1.2(a), also known as the phase diagram, represents the three phases domains and reveals the sublimation, fusion, and vaporization curves corresponding to the solid-vapor, solid-liquid, and liquid-vapor equilibrium lines, respectively, which move from left to right. These three curves converge at the triple point, where the three phases coexist in equilibrium.

The critical point, also called the critical state, marks the limit beyond which liquid and vapor can no longer coexist. It is where the vaporization curve terminates; beyond the pressure corresponding to the critical point, the transition from vapor to liquid occurs smoothly without the two phases coexisting.

In Figure 1.2, the p−v and p−T diagrams of a typical substance are presented (not to scale). Figure 1.3 shows an isotherm that depicts a phase transition (also not to scale).

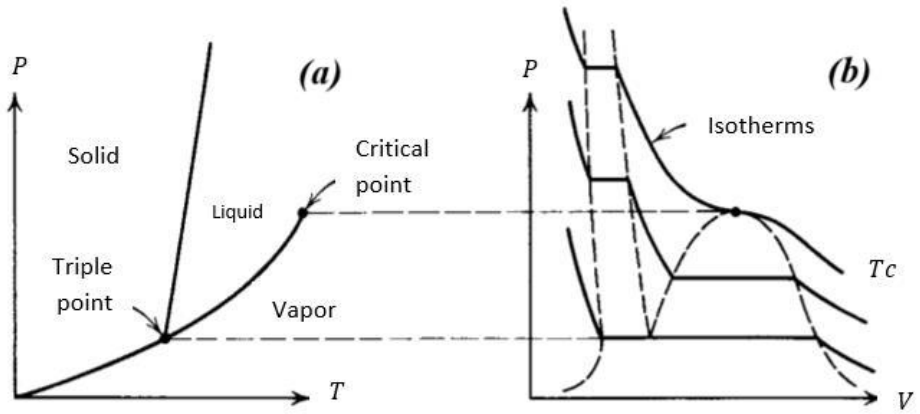

***Figure 1.2**. $p-T$ **(a)** and $p-V$ **(b)** diagram of a pure substance* [5]

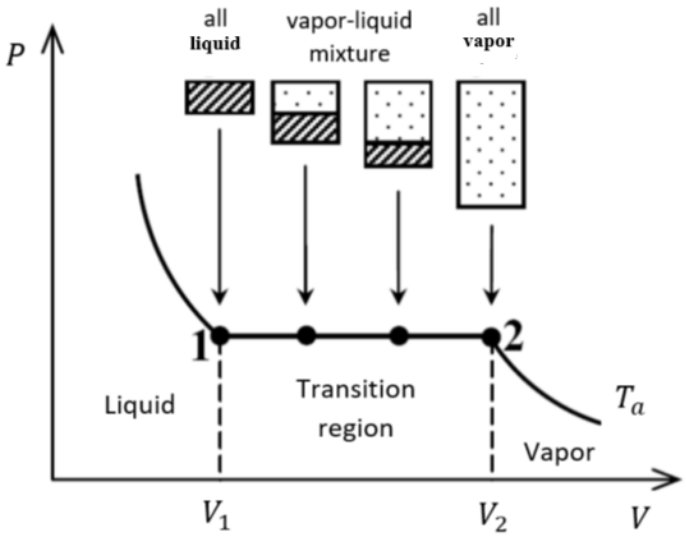

***Figure 1.3**. State transition represented in a p-V diagram corresponding to an isotherm* [6]

For example, in the transition between liquid and vapor, as shown in Figure 1.3, the phase change occurs at constant temperature and pressure. This pressure $p(T)$ is referred to as the vapor pressure at temperature T. Initially, the system is entirely liquid in state 1. As heat is introduced, some liquid converts to vapor, shifting the state to the right on the graph until the system reaches state 2, where it becomes entirely vapor. During the phase transition, pressure and temperature remain unchanged. In the liquid-vapor mixture, the liquid remains in the same state as in state 1, and the vapor exists in the same state as in state 2.
In cases of polymorphism (or allotropism)[7], the $p{-}v{-}T$ diagram becomes more complex, as different solid forms of the same substance can exist. This introduces new single-phase regions, additional equilibrium lines, and more triple points. An example of this is the phase diagram of sulfur at low pressures, which shows two solid phases, rhombic and monoclinic, resulting in three triple points: rhombic-monoclinic-vapor, monoclinic-gas-liquid, and rhombic-monoclinic-vapor [8].

1.3 State functions

In thermodynamics, a state function is a mathematical expression that represents some thermodynamic property of a system in equilibrium. State functions depend solely on the current state of the system, rather than the process or path taken to reach that state. In other words, they are independent of transformations done, they depend only on the state at the start of the process and the end of the process [9].

To calculate a state function, it is possible to use a hypothetical and ideal route to reach some final state, even if real processes typically occur through out-of-equilibrium stages. Some of the most used state functions include entropy (S), enthalpy (H), and Gibbs free energy (G) [10].

Enthalpy, *H*, is defined as the heat content of a chemical or physical system plus the product of its pressure and volume:

$$H = U + pV \qquad \text{Eq. 1.2}$$

In Eq. 1.2, the term *U* represents the system's internal energy, while pV accounts for the volume work done on or by the system required for establishing and positioning itself. Internal energy, which represents the energy required to create a thermodynamic system, consists of two components: kinetic energy and chemical potential energy.

Entropy, *S*, is a thermodynamic quantity, an extensive property, and a measure of the amount of thermal energy in a system that is unavailable for doing work. It is a fundamental concept derived from the second law of thermodynamics. It also serves also as a macroscale indicator of the degree of molecular disorder within a system, as expressed by Boltzmann equation [11]:

$$S = k\, lnW \qquad \text{Eq. 1.3}$$

Where *k* is Boltzmann's constant and *W* the number of state accessible to the system.

The change in entropy between two states depends solely on the initial (1) and final (2) states of a reversible process:

$$\Delta S = S_2 - S_1 = \int_1^2 \frac{\delta Q}{T} \qquad \text{Eq. 1.4}$$

where δQ represents the reversible heat flux and T is the absolute temperature.

For a first-order phase transition (discussed in Section 1.4), the reversible heat flux is equivalent to the heat exchanged at constant temperature and pressure, which in turn corresponds to the enthalpy change during the transition. Hence, the entropy change for a first-order phase transition is given by:

$$\Delta S = S_2 - S_1 = \frac{H_2 - H_1}{T_{12}} = \frac{\Delta H}{T_{12}} \qquad \text{Eq. 1.5}$$

Where ΔH is the enthalpy change during the transition from phase 1 to phase 2, and T_{12} is the transition temperature at a specified pressure.

Gibbs free energy, *G*, is a thermodynamic potential that is measure of the maximum available work that can be derived from any system, specifically, when a process occurs under conditions of constant pressure and temperature [9]. It is defined as

$$G(p,T) = U + pV - TS = H - TS \qquad \text{Eq. 1.6}$$

Where *U* is the internal energy, *H* is the enthalpy, *S* the entropy and *p*, *T* are pressure and temperature.
By expressing the Gibbs energy in its differential form

$$dG = dU + pdV + Vdp - Tds - SdT \qquad \text{Eq. 3.7}$$

And considering that, by the first law of thermodynamics, $dU = TdS - pdV$, then the differential of Gibbs energy is equal to

$$dG = Vdp - SdT \qquad \text{Eq. 1.8}$$

Representation through differentials of a function $f = f(x, y)$ is done through its partial derivatives with respect to each variable:

$$df = \frac{\partial f}{\partial x}dx + \frac{\partial f}{\partial y}dy \qquad \text{Eq. 1.9}$$

Thus, from Eq. 1.8, it can be written:

$$\left|\frac{\partial G}{\partial p}\right|_{T=cost} = V \qquad \text{Eq. 1.10a}$$

$$\left|\frac{\partial G}{\partial T}\right|_{p=cost} = -S \qquad \text{Eq. 1.10b}$$

That is, the volume is the partial derivative of Gibbs energy with respect to pressure at constant temperature, and entropy is the opposite of the partial derivative of Gibbs energy with respect to temperature at constant pressure [9].

Gibbs energy function can be referred to each separate phase *i* that comprises a thermodynamic system, across all ranges of temperature and pressure. This functions $G_i(p, T)$ are typically represented in a three-dimensional cartesian plane, where two axes are the thermodynamic variables *p*, *T* and the other is the thermodynamic potential G_i (or g_i). Then, all the possible values that the functions can assume lay on two-dimensional surfaces. A visual representation (in massic terms) is given in Figure 1.4.

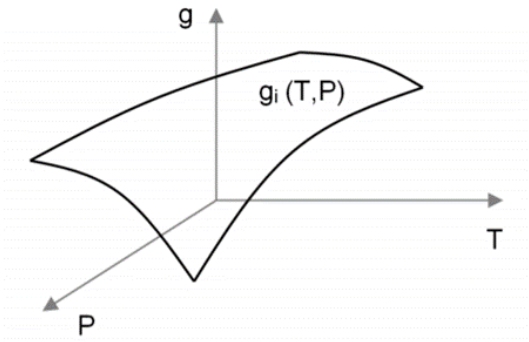

***Figure 1.4**. Surface g(p, T) for a given phase* i [12]

It's well established that at given equilibrium state, at constant *p*, *T*, the phase with the minimum *G (p, T)* value is defined as the stable phase.

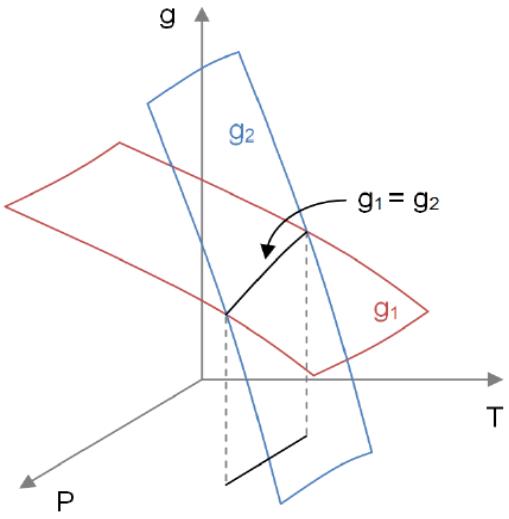

***Figure 1.5**. Surfaces* g(p T) *for two phases,* g_1 *and* g_2*, showing a coexistence domain at* $g_1=g_2$ [12]

In Figure 1.5, intersecting Gibbs functions corresponding to phases *1* and *2*, g_1 and g_2, are represented for the same range of values p, T. For a certain subset of p, T values the function g_1 assumes smaller values than g_2 ($g_1<g_2$); then, phase *1* is the stable phase, while phase *2* is defined as a metastable phase. For another subset of p, T values, instead, the function g_2 is the one that has smaller values than g_1 ($g_1>g_2$); in this domain, phase *2* is the stable phase while phase *1* is the metastable phase. One important observation is that, for some p, T value, only one stable phase can exist, while there can be multiple metastable phases.

In the next paragraph the case of $g_1 = g_2$ will be explained, that is, when equilibrium between two phases subsists.

1.4 Clausius-Clapeyron equation. Phase equilibrium conditions

Given that systems achieve equilibrium at a specified temperature T and pressure p, when the Gibbs energy reaches a minimum, let the moles of the first phase be n_1 and those of the second phase be n_2. If the system is in equilibrium at the given temperature T and pressure $p(T)$, the Gibbs energy in this state must be minimized. Specifically, if parameters other than T and p are slightly altered, then $dG = 0$ must hold, as established earlier. Altering the mixture's composition by converting an amount ∂n from the first phase to the second, while conserving the number of particles ($n_1 + n_2 = n$), results in the following equation:

$$-\partial n_1 = \partial n_2 = \partial n \qquad \text{Eq. 1.11}$$

The total Gibbs energy of the mixture can be expressed as:

$$G(p,T) = n_1 g_1(p,T) + n_2 g_2(p,T) \qquad \text{Eq. 1.12}$$

Here, g_1 and g_2 represent the molar Gibbs energy for the distinct phases involved, also known as chemical potential μ (μ_1 and μ_2, respectively). These are independent of the total phase mass but may depend on phase density, though phase density does not change when transitioning between phases. Thus:

$$dG = -(g_1 - g_2)dn = 0 \qquad \text{Eq. 1.13}$$

The equilibrium condition ($dG = 0$) is therefore:

$$g_1(p,T) = g_2(p,T) \qquad \text{Eq. 1.14}$$

By expressing Eq. 1.10a and 1.10b in molar terms

$$\left(\frac{\partial g}{\partial p}\right)_T = v \qquad \text{Eq 1.15a}$$

$$\left(\frac{\partial g}{\partial T}\right)_p = -s \qquad \text{Eq 1.15b}$$

Most of phase transitions found belong to a class called first-order phase transitions. These transitions are characterized by the presence of a latent heat of transition, as well by the discontinuity in state variables such as entropy and molar volume. If the phase transition 1-2 is of the first order, then it can be written:

$$\left(\frac{\partial g_2}{\partial p}\right)_T - \left(\frac{\partial g_1}{\partial p}\right)_T = v_2 - v_1 \qquad \text{Eq. 1.16a}$$

$$\left(\frac{\partial g_2}{\partial T}\right)_p - \left(\frac{\partial g_1}{\partial T}\right)_p = -(s_2 - s_1) \qquad \text{Eq. 1.16b}$$

The discontinuity is also present in the first order derivatives of the Gibbs function (hence the name). Figure 1.5 shows the Gibbs free energy curve at transition pressure (Fig. 1.5a) and temperature (Fig. 1.5b). Similarly, Figure 1.6 depicts a *S(T)* diagram showing the discontinuity of entropy at first-order phase transition.

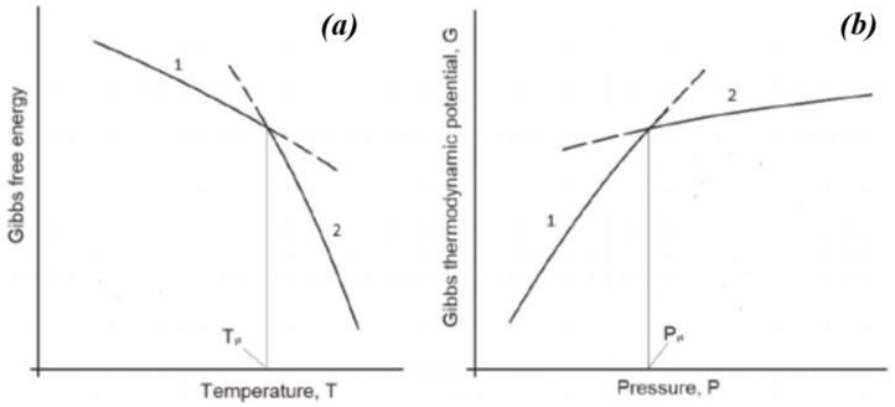

***Figure 1.5**. Gibbs free energy in respect to temperature (while p=cost.) **(a)** and pressure (while T=cost.) **(b)** at a first-order transition [13]*

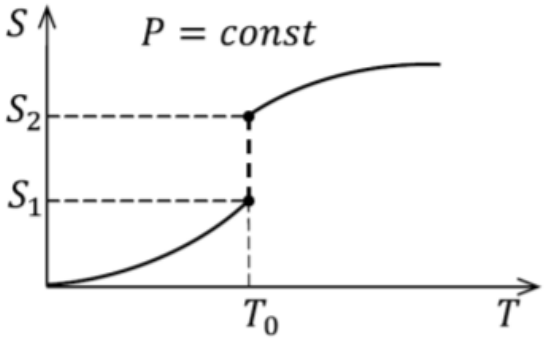

***Figure 1.6**. Entropy discontinuity at a first order transition* [6]

At equilibrium, the conditions for T and p must make $\Delta g = 0$. By dividing Eq. 1.16b by Eq. 1.16a, we find:

$$\frac{\left(\frac{\partial \Delta g}{\partial p}\right)_T}{\left(\frac{\partial g_2}{\partial T}\right)_p} = -\frac{\Delta s}{\Delta v} \qquad \text{Eq. 1.17}$$

The discontinuities Δg, Δs, and Δv are functions of v, T, and p, which are related through the state equation $f(p, v, T) = 0$. Then, a function must exist such that $f(T, p, \Delta g) = 0$. By using the chain rule:

$$\left(\frac{\partial \Delta g}{\partial T}\right)_p \left(\frac{\partial T}{\partial p}\right)_{\Delta g} \left(\frac{\partial p}{\partial \Delta g}\right)_T = -1 \qquad \text{Eq 1.18}$$

Alternatively:

$$\frac{\left(\frac{\partial \Delta g}{\partial T}\right)_P}{\left(\frac{\partial \Delta g}{\partial p}\right)_T} = -\left(\frac{\partial p}{\partial T}\right)_{\Delta g} \qquad \text{Eq. 1.19}$$

The chain rule is applicable because Δg is a function of T and p. Since both temperature and pressure are state variables, it can be written that, at equilibrium:

$$\frac{dp(T)}{dT} = \left(\frac{\partial p}{\partial T}\right)_{\Delta g} \qquad \text{Eq. 1.20}$$

By combining Eq. 3.17 and Eq. 3.20

$$\frac{dp(T)}{dT} = -\frac{\Delta s}{\Delta v} \qquad \text{Eq. 1.21}$$

Remembering that at transition temperature entropy and enthalpy are related through Eq. 1.5, it's possible to finally write

$$\frac{dp}{dT} = \frac{\Delta s}{\Delta v} = \frac{\Delta h}{T \Delta v} \qquad \text{Eq. 1.22}$$

Here, ΔH is the latent heat associated with the phase transition at temperature T under constant pressure. In any phase transition accompanied by entropy changes, if the process occurs at constant pressure, then the (latent) heat is equivalent to the enthalpy change during the transition:

$$\frac{dp}{dT} = \frac{\Delta h}{T\Delta v}$$ Eq. 1.23

This is the Clausius-Clapeyron equation [3], which gives the variation of pressure with temperature along the transition line. For endothermic processes, heat is required for the transition to proceed (thus, $\Delta h > 0$), while the opposite is true for exothermic processes, as heat is released during the transition, heating the surroundings ($\Delta h < 0$).

2. Solid-solid phase transitions

2.1 Polymorphism

Polymorphism is a term used in both biology and crystallography to describe the ability of molecular compounds to exist in multiple solid forms with distinct chemical and physical properties. In simpler terms, this occurs when a chemical substance crystallizes in different structures, which is determined by the processes of nucleation and growth. In the solid state, the molecular units, known as the system's asymmetric units, can arrange themselves into one of seven basic crystalline forms: monoclinic, triclinic, orthorhombic, tetragonal, trigonal, hexagonal, and cubic.

Typically, polymorphs of a particular compound can differ as much in structure and properties as crystals of completely different substances. Characteristics such as solubility, hardness, density, melting point, crystal shape, electrical and optical properties and vapor pressure all vary with the polymorphic form. This diversity in crystal forms enables the possibility of modifying the performance characteristics of a compound by obtaining different crystalline versions of it.

As a result, in recent decades, interest in polymorphic systems has significantly increased, particularly in their role in developing and marketing a wide range of materials based on organic molecules. Moreover, the variation in properties between different polymorphs has attracted significant attention from pharmaceutical scientists due to their potential impact on formulation, manufacturing, and drug bioavailability. In these cases, regulatory considerations can become crucial and influence the development pathway for a particular pharmaceutical compound, leading to the rise of a specialized field of characterization techniques for assessing pharmaceutical solids. Interestingly, a substantial number of pharmaceutical compounds exhibit polymorphism. It has been found that 60% of barbiturates, 70% of sulfonamides, and 25% of hormones exist in different polymorphic forms [14]. Well-known anti-inflammatory drug nimesulide was characterized by Barrio *et al*.[15] in a similar manner to the compound here studied, and it was found that one polymorphic form was more stable and thus better suited for pharmaceutical formulations. While orcinol itself is not a medical drug, a known co-crystal, orcinol glucoside, is an important antidepressant [16, 17] and was found to promote osteogenesis and prevent osteporosis[18]. So, even if the data later presented does not have significant pharmaceutical interest, any possible drug involving orcinol as a part of a co-crystal will likely have to be characterized similarly to how was done in this work.
Strictly speaking, polymorphs must maintain the same chemical composition. This is why hydrates or solvates are referred to as pseudo-polymorphs. Polymorphs can be categorized into two main subtypes [19]:

- *Conformational polymorphism*: this occurs when molecules with different conformations exist in the crystalline state. This type of polymorphism is quite common, especially in pharmaceutical compounds that generally contain flexible structures within their molecular framework;
- *Packing polymorphism*: here, the molecules have the same molecular conformation but are arranged differently in three-dimensional space.

2.2 Stability and metastability

Under certain conditions, within a specific range of pressure and temperature, one polymorph can transform into another that is more thermodynamically stable. Polymorphs differ due to their distinct crystal lattices, which affect their lattice energies. If two solid forms exist at a given temperature and pressure, the form with the higher Gibbs free energy is considered metastable at those conditions, while the form with the lowest Gibbs free energy is identified as the more stable one.

The stability of each form is governed by thermodynamic laws. At a given temperature and pressure, only one polymorphic form will be physically stable, while the others will be metastable. A hierarchy of stability can thus be established. If multiple forms exist at the storage temperature, the less stable form (with higher g) will tend to convert into the more stable one (with lower g). Regardless of the medium (except for solvates or hydrates), metastable forms usually transition to a more stable state, but this transformation only begins after the first nuclei of the stable polymorph appears [21].

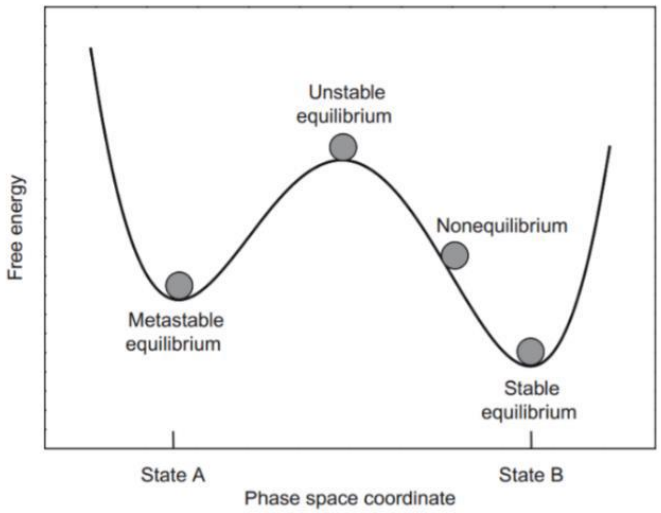

***Figure 2.1**. Illustration of equilibrium and non-equilibrium states [22]*

Figure 2.1 offers a good example of this, illustrating free energy as a function of generalized coordinates that describe the transition from state *A* to state *B* (coordinates sign is positive when moving from the initial to the final state).
The relation between polymorphs is generally divided into enantiotropic or monotropic classes, based on their thermodynamic properties. In an enantiotropic relationship, the transition between polymorphs is reversible at a specific temperature and pressure below the melting point [23] (Figure 2.2b). In contrast, a monotropic relationship shows no reversible transition between the polymorphs below the melting point [24] (Figure 2.2a).

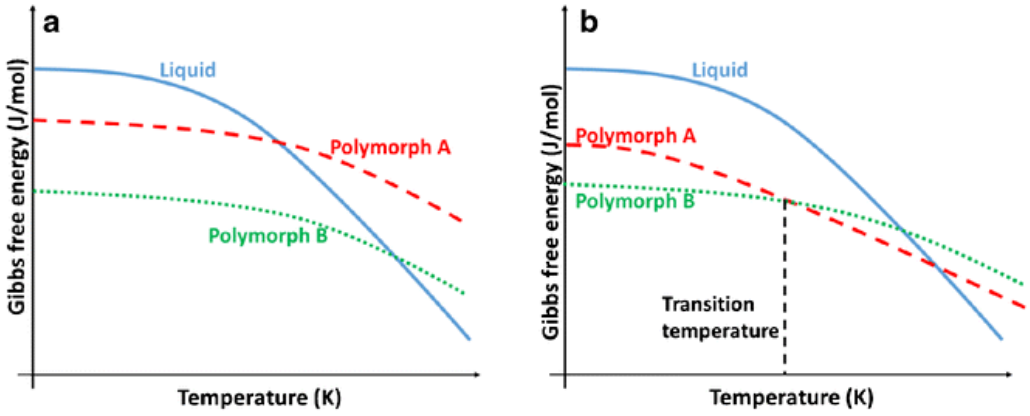

***Figure 2.2**. G(T) diagrams at costant pressure, depicting Gibbs energy of monotropically related (**a**) and enantiotropically related (**b**) polymorphs* [25]

This classification will be further detailed in Section 2.3 regarding stability hierarchies.

2.3 Stability hierarchies

Burger and Ramburger outlined various guidelines to qualitatively determine whether the relationship between polymorphs is monotropic or enantiotropic. While some of these guidelines are based on common behaviors, not all are grounded in fundamental thermodynamic principles, so they should be applied cautiously. Nevertheless, many of these guidelines are widely used, and thus they are outlined below. Three particularly useful rules they proposed are the heat of transition, heat of fusion, and density rule. The first two require calorimetric measurements, commonly performed using DSC [26]. As for the density rule, specific volumes can be determined through X-ray diffraction techniques.

In general, thermodynamic relationships can be experimentally evaluated by calculating the Gibbs free energy difference between polymorphs over temperature ranges through direct heat capacity measurements [19].

Thermodynamic guidelines for determining the relative stability and relationships of dimorphic systems [27]:

- *Heat of transition rule*:
  If an endothermic transition from the lower melting form to the higher melting form is observed, the forms are enantiotropic. If an exothermic transition occurs, the polymorphs are monotropic or the transition temperature is higher.
- *Heat of fusion rule*:
  Polymorph pairs are enantiotropically related if the higher melting form has a lower heat of fusion. Otherwise, they are monotropic.
- *Entropy of fusion rule*:
  Polymorphs are enantiotropic if the higher melting form has a lower entropy of fusion; otherwise, they are monotropic.
- *Heat capacity rule*:
  Polymorphs are enantiotropically related if the higher melting form has a higher heat capacity at a given temperature than the other polymorph.
- *Density rule*:

The polymorph with the higher density, assuming no directional intermolecular interactions, is more stable at 0 K than the polymorph with lower density.

- *Infrared rule*:

A polymorph with the highest frequency infrared absorption band of a hydrogen-bonded molecular crystal may be assumed to have greater entropy than one with a lower absorption band.

- *Solubility rule*:

Polymorphs are enantiotropic if the higher melting form has greater solubility above the transition temperature. In monotropic systems, the higher melting form will have lower solubility.

The Gibbs free energy isobars can follow different paths, and their intersections represent transition points between phases. Burger (1951) suggested the possibility of two isobars crossing twice, but Burger and Ramburger (1979) used statistical-mechanical arguments to show that only one crossing is physically possible, since Gibbs energy is a monotonous function of temperature and pressure.

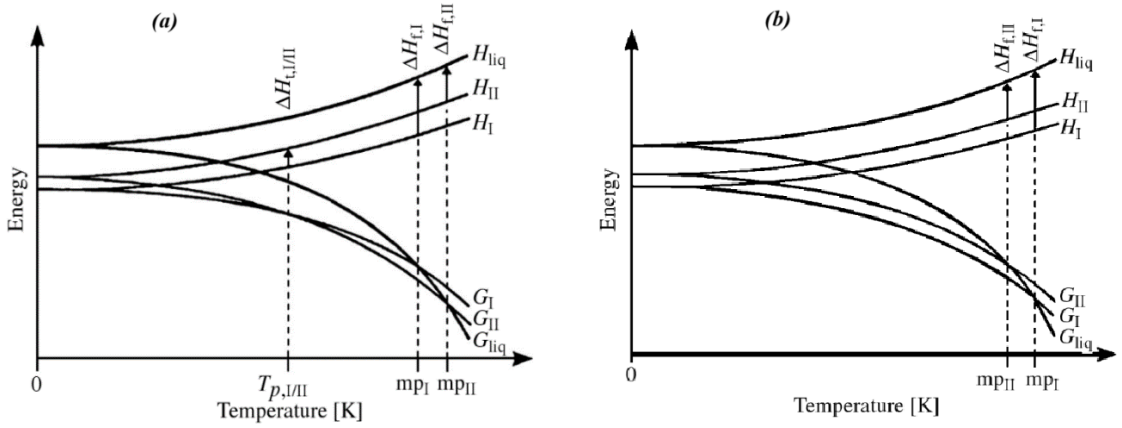

***Figure 2.3**. Plot of Gibbs energy and enthalpy from absolute zero to transition temperatures of enantiotropically related (**a**) and monotropically related (**b**) polymorphs* [27]

Figure 2.3 illustrates the energy versus temperature diagram for a dimorphic system at a given pressure. On the left, an enantiotropic phase relationship is shown where Form I is stable below the transition point. On the right, a monotropic phase relationship is depicted, where Form I is more stable across all temperatures.

In summary, polymorphs of a given substance can have either monotropic or enantiotropic phase relationships. The thermodynamically stable or metastable domain of each crystalline phase can be defined as a function of temperature and pressure.

2.4 Crystal dimorphism: four possible cases

In 1901, Bakhuis-Roozeboom demonstrated that only four types of pressure-temperature phase diagrams are possible for crystalline dimorphism [29]. Prior to this, in 1891, Lehmann had defined enantiotropy as a process in which one form (Form I) transforms into another (Form II) with increasing temperature, and reverts back to the first form as the temperature decreases. Enantiotropy indicates that both solid forms can change reversibly between each other and maintain stability under

normal conditions. Lehmann defined monotropy as a scenario where Form I transforms into Form II with increasing temperature, but does not revert back to Form I when the temperature is lowered. From a purely thermodynamic perspective (ignoring slow or hindered transformations), in this case, Form II would be the stable form across the entire temperature range, making Form I monotropic in relation to Form II.

When pressure is introduced as an additional factor, the pressure-temperature phase diagrams described by Bakhuis-Roozeboom, shown in Figure 2.4, can be obtained. The system can remain monotropic (as illustrated in Figure 4.4(1)), showing then overall monotropy. If the system remains enantiotropic (Figure 2.4(2)), the compound shows overall enantiotropy. Two additional situations can be obtained, the system change from monotropic to enantiotropic behavior at higher pressure (Figure 2.4(3)), or switch from enantiotropic to monotropic with increasing pressure (Figure 2.4(4)). These transitions are determined by the position and slope of the two-phase equilibria involved.

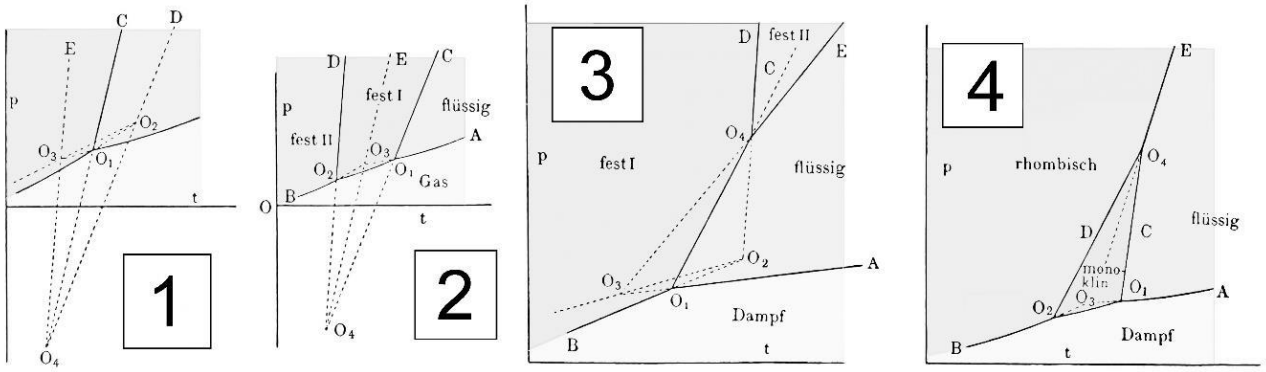

***Figure 4.4**. Four different p(T) diagrams according to Bakhuis-Roozeboom: **(1)** complete monotropy, **(2)** complete enantiotropy, **(3)** a monotropic system becoming enantiotropic at high pressure, and **(4)** an enantiotropic system becoming monotropic at high pressure* [30]

For systems involving trimorphism, tetramorphism, or higher levels of polymorphism, phase diagrams become more complex. However, because stability is defined by the Gibbs free energy surfaces as a function of temperature and pressure, it is possible to study all polymorphs in relation to one other polymorph within the same system. Enantiotropic and monotropic relationships can always be established between any two polymorphs. Additionally, a polymorphic phase diagram can be understood as a superimposition of individual dimorphic diagrams as described by Bakhuis-Roozeboom. This means that even if a polymorphic phase diagram is complex, it can be simplified into a series of dimorphic diagrams, making the analysis more manageable [30].

3. Instrumentation and techniques

The techniques utilized to characterize the physical states that orcinol can assume were mainly thermal analytic techniques. This class of techniques makes it possible to measure several thermodynamic quantities such as transition enthalpy, transition temperature, specific heat capacity, glass transition temperature. Other than that, XRD experimental setup is crucial to determine the physical state of a certain solid as well as its crystal structure (if present).

3.1 Thermal Analysis Techniques

Thermal analysis comprises a group of techniques in which a physical property of a substance is measured as a function of temperature, while the substance is subjected to a controlled temperature program. In the classical DTA and their subtle modification the heat–flux DSC the temperature difference developed between a sample and an inert reference material is measured when both are subjected to the same heat flux.

3.1.1 Heat-flux differential scanning calorimetry (DSC)

In heat-flux DSC, sample and reference are connected by a low-resistance heat-flow path (a metal disc). The assembly is enclosed in a single furnace that can be submitted to heating and cooling ramps. Enthalpy or heat capacity changes in the sample cause a difference in temperature relative to the reference, and this temperature difference is recorded and related to enthalpy change in the sample using calibration experiments [32].

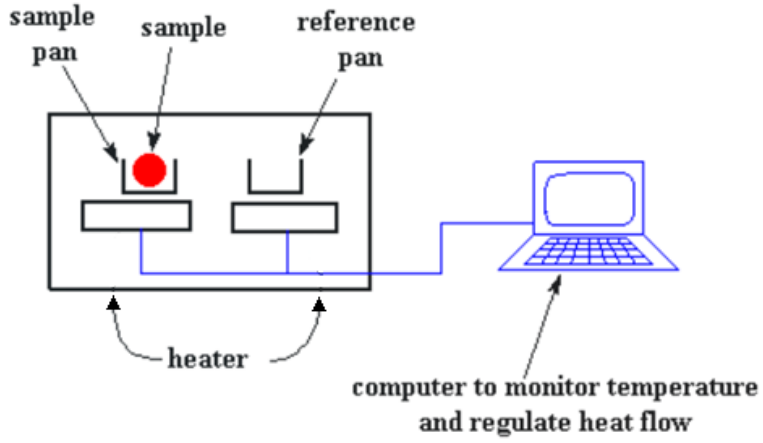

***Figure 3.1**. Schematic representation of the main components of a DSC [33]*

The signal obtained in these systems is called a thermogram (Figure 3.2). This signal is a plot of the differential temperature (or power) as a function of time or temperature (assuming that heating rate is known).

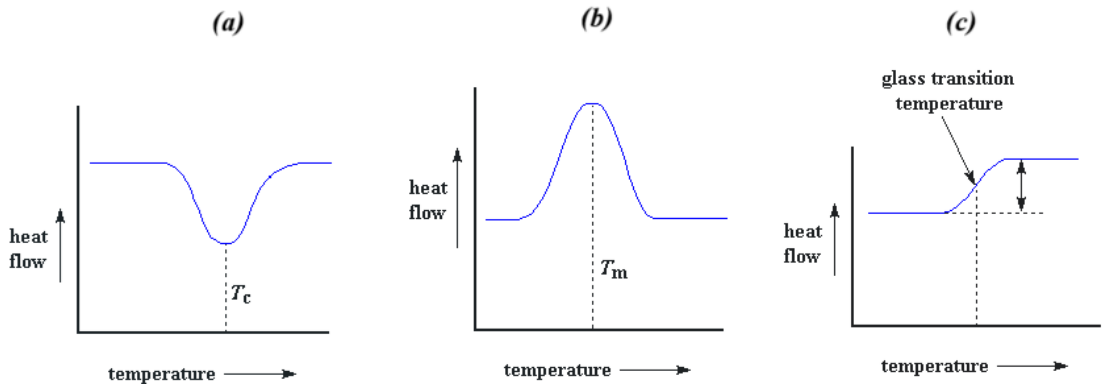

***Figure 3.2**. Thermograms depicting different transition phenomena: exothermic transition (**a**), endothermic transition (**b**) and glass transition (**c**)* [34] .

However, the transition temperature is not the temperature corresponding to the maximum of the peak, as Figure 3.2 might suggest. An endothermic event, as could be the melting of the sample, yields a peak on the DSC signal, Figure 3.3. The initial peak temperature, T_i, is the temperature (at time t_i) where the curve begins to deviate from the initial base line; the final temperature, T_f, is the temperature (at the time t_f) where the curve reaches the final baseline. The interpolated base line between these temperatures will be a horizontal straight line if the capacities of the solid and liquid phases are very similar. The temperature T_O where the extrapolated ascending peak slope intersects the extrapolated initial base line is the extrapolated peak onset temperature. By convention, T_O is the transition temperature. The area of the peak defined by the interpolated baseline and the peak is proportional to the enthalpy of transition, ΔH_{tr}. The enthalpy calibration allows to establish the relationship between the enthalpy change measured (peak area ΔH_{meas}) by the instrument for a given transition, and the true transition enthalpy change of the sample: $\Delta H_{tr} = K \cdot \Delta H_{meas}$, being K the constant calibration [35].

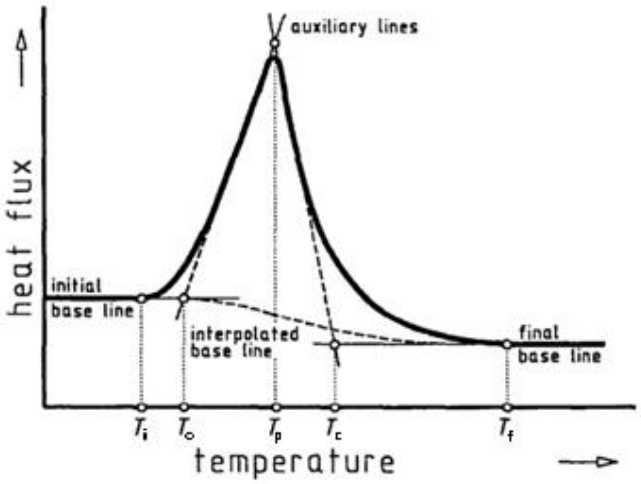

***Figure 3.3**. Plot of heat flux versus temperature (thermogram) of an endothermic transition of a pure substance* [35]

Figure 3.4 shows the possible DSC plots that could arise when dealing with polymorphs that are monotropically related (Fig. 3.4(a)) or enantiotropically related (Fig. 3.4(b)).

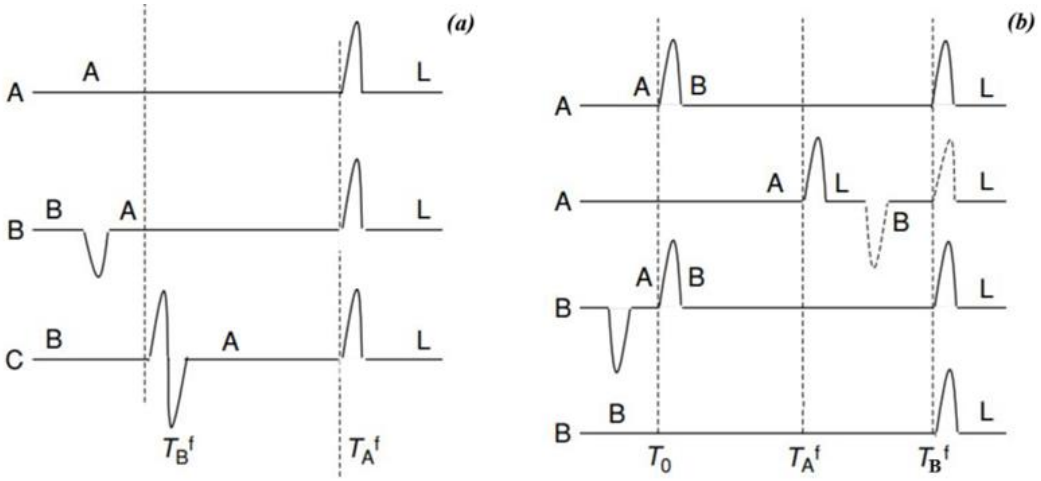

***Figure 3.4**. Possible thermograms of (**a**) monotropic dimorphs and (**b**) enantiotropic dimorphs* [36]

The device used in this work was TA Instruments DSC Q100. This instrument can work from -70 °C to 600 °C. Scanning rates between 2 to 10 ºC/min have been used in the cooling and heating ramps. The samples, between 3-10 mg, have been encapsulated in aluminum pans.

3.1.2. High pressure differential thermic analysis (HP-DTA)

The operating basis of this device is the same as that of the DSC. Sample and the reference are placed symmetrically in the furnace and can been submitted at different pressures ranged between normal pressure and 300 MPa. The furnace is controlled under a temperature program and the temperature of the sample and the reference are changed. During this process, a differential thermocouple is set up to detect the temperature difference $\Delta T = T_S - T_R$ where T_S and T_R the temperature of the sample and the reference, respectively. Also, the sample temperature is detected from the thermocouple on reference side [37].

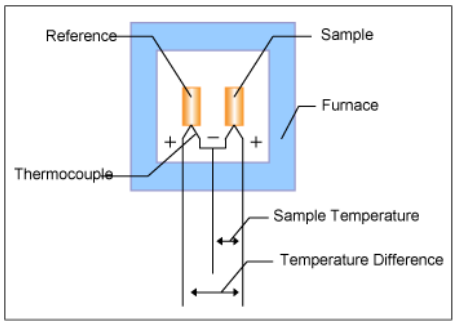

***Figure 3.5**. Schematic representation of the components of a DTA [38]*

When the furnace heating begins, the reference and the sample heat with a slight delay depending on their respective heat capacity, and eventually heat up according to the furnace temperature. Temperature difference until a static state is reached after the heating begins, and after achieving stability, reaches a set amount compliant with the difference in heat capacity between the sample and the reference. The signal at the static state is known as the baseline.

When the temperature rises and melting occurs in the sample, for example, the rise of sample temperature T_S stops while T_R increases, as shown in Figure 3.6(a). When the melting ends, the temperature curve rapidly reverts to the baseline. During this point, the ΔT signal reaches a peak, as shown in Figure 3.6(b).
From this, we can detect the transition temperature from the ΔT signal (DTA signal).
In Figure 3.6(b), the temperature difference due to the samples endothermic change is shown as a negative direction and the temperature difference due to the samples exothermic change is shown as a positive direction.
Thermograms obtained by DTA are expressed as temperature difference ΔT versus time (or temperature).

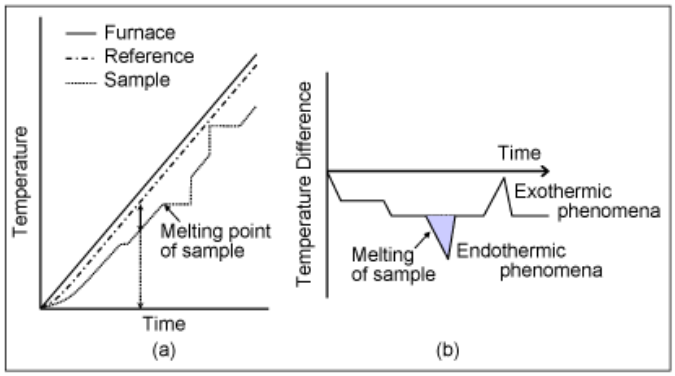

***Figure 3.6**. (**a**) Evolution of temperature as time increases of furnace, reference and sample; (**b**) usual depiction of a DTA thermogram* [38]

Pression on the sample is exerted by a liquid that is introduced from a reservoir to a pump that can compress up to 300 MPa. This high-pressure liquid is transferred to the calorimetric system which holds the sample through a capillary system. Manganin manometer allows to know the pressure at which the sample lies. The instrument utilized in this study was devised by the GCM (Group Characterization of Materials) research group at Universitad Politecnica de Catalunya on the basis of a work of Würflinger [39]. This instrument allows thermograms to be obtained at different pressures, in the range 1-3000 bar. Crucible for HPDTA were hand-made by casting melt tin (Sigma-Aldrich, CAS 7440-31-5) into a steel mold. Galden ® HT270 (CAS 69991-67-9), a heat transfer fluid, was utilized in order to avoid having air inside the crucible that would falsify the measurements.

3.1.3. Thermogravimetric analysis (TGA)

Thermogravimetric analysis (TGA) is a thermal analytic technique commonly utilized in chemistry and engineering. It registers the weight variation of a sample as a function of temperature by means of a microbalance, on which the sample is placed or attached. Balance and sample are both placed inside a furnace. Figure 3.7 gives a representation of a TGA setup.

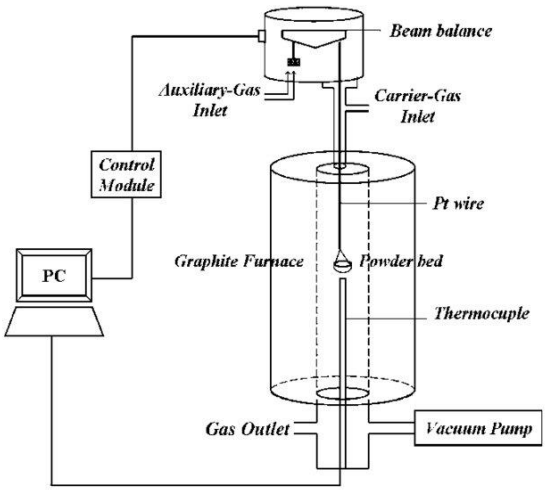

Figure 3.7. *Schematic representation of a TGA experimental setup* [40]

The instrument allows to heat up the sample following pre-programmed heating runs. In particular, the TGA can be conducted in three different modalities:

- Dynamic TGA - Temperature continues to increase over time as mass is recorded. This allows simultaneous identification of how much gas is removed and the temperature at which it occurs.
- Static TGA - Temperature is held constant as the mass is measured. This can be used to gain more information on a decomposition that happens at a certain temperature or to investigate a material's ability to withstand a given temperature.
- Quasistatic TGA - Sample is heated in multiple temperature intervals, and held at those intervals for a time, often until the mass stabilizes. This is ideal for investigating substances that are known to decompose in various ways at different temperatures, and better characterizing the way in which they decompose.

While the sample is continuously heated an inert gas atmosphere is passed over it. Many solids undergo reactions that evolve gaseous byproducts. In TGA, these gaseous byproducts are removed and changes in the remaining mass of the sample are recorded.

When heating, depending on the phenomenon at play, the weight could increase (absorption of environmental gases) or decrease (degradation reaction of the sample).
The weight of the sample is registered through time and plotted in a graph against temperature (or time). Alternatively, the weight variation rate (weight over time) can be plotted against temperature (or time) (which corresponds to the time derivative, for this reason is indicated as DTG) [41]. Examples of both can be seen in Figure 5.8.

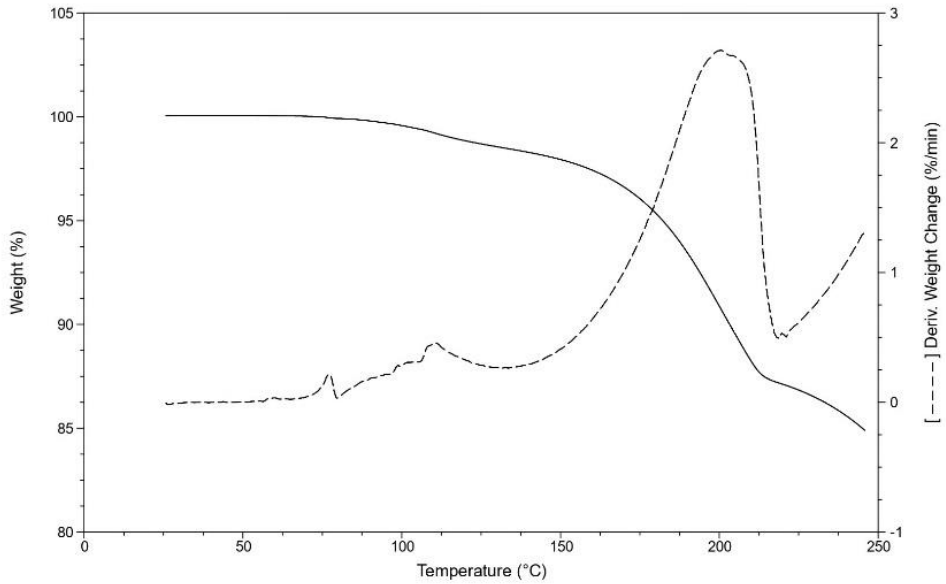

***Figure 3.8**. TG and DTG plot. The continuous line is weight (in %) versus temperature, while the dotted line is the weight change (in %/min) versus temperature*

While the working principle is simple (extremely precise microbalance), the actual setup requires routine checks and calibrations.
The main parts are:
- analytic balance with sensitivity in the order of micrograms
- sample holder
- furnace (temperatures usually in the range from 25 °C to 1500 °C)
- flux system of purge gas, to avoid deposition of degradation byproducts on the sample itself
- control system that acquires data

The instrument utilized in this work was TA Instruments TGA Q50. Samples were prepared by putting 3-10 mg of orcinol powder in an aluminum pan. Heating rates were held at 10 °C/min.

3.2 X-ray diffractometry

X-ray diffractometry (XRD) is a fast, effective, non-destructive technique mainly used to characterize crystalline materials. It provides crucial data on structures, phases, preferred crystal orientations (textures), and other structural features, including average grain size, crystallinity, strain, and crystal defects [42]. As a technique, it permits to investigate the physical structure of a solid phase. Experimental evidence shows that crystalline solids (both single crystals and crystal powder), when incised by X-rays, will form a regular pattern of spots on a photographic plate, both by reflection and diffraction with the ordered periodic lattice of a crystal. The interaction of the X-ray beam with the sample leads to constructive interference when the conditions meet Bragg's law [43]:

$$n\lambda = d \sin\theta \qquad \text{Eq. 3.1}$$

where n is the diffraction order, λ is the X-ray wavelength, d is the interplanar spacing, and θ is the diffraction angle. Figure 3.9 shows a schematic representation of a scenario where Bragg's law is applicable.

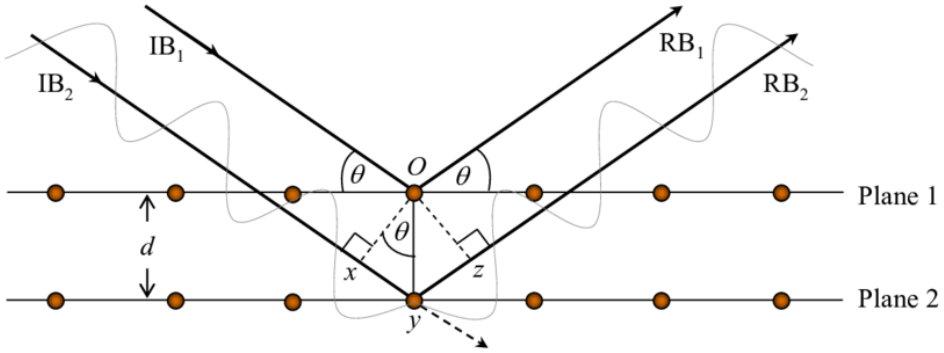

***Figure 3.9**. Schematic representation of X-ray waves interaction with two crystalline planes. Plane distance, wavelength and incident angle are related by Bragg's law* [44]

By scanning the sample through a range of 2θ angles, all possible diffraction directions of the lattice are obtained due to the random orientation of the powdered material, see Figure 3.10. Then the X-ray diffraction peaks in a diffractogram, see Figure 3.11, arise from the constructive interference of a monochromatic X-ray beam scattered at specific angles from different sets of lattice planes in the sample.
The experimental pattern is called a diffractogram. An example of it is found in Figure 3.11.

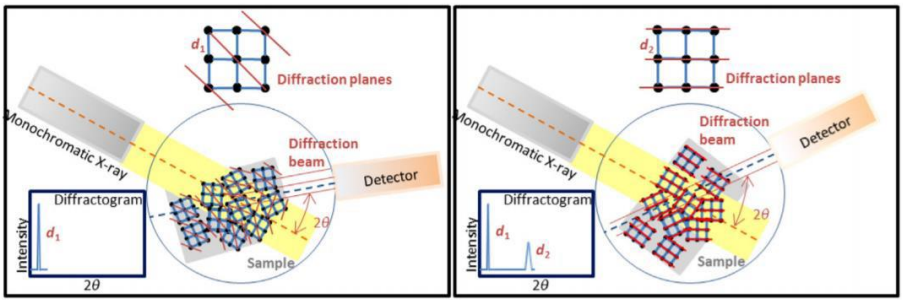

***Figure 3.10**. Generation of the powder pattern by a diffractometer* [45]

.

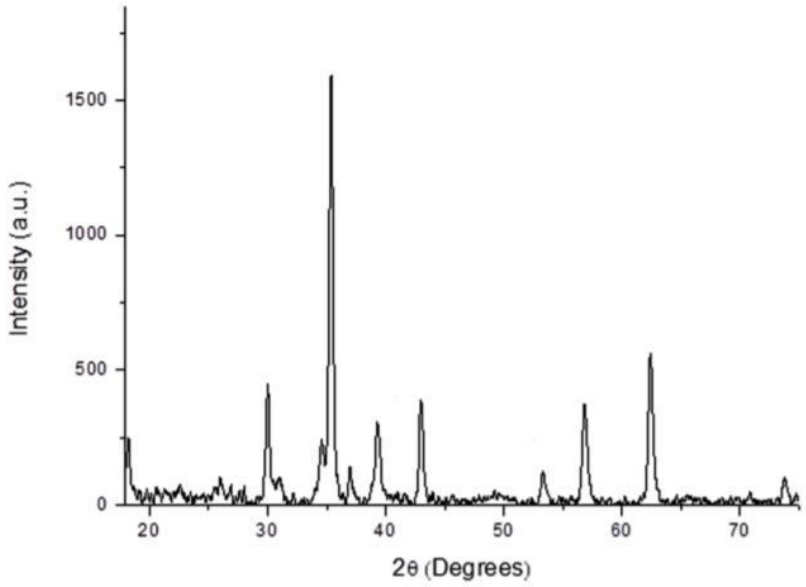

***Figure 3.11**. Diffractogram showing intensity as a function of the angle θ*

The intensity of the peaks depends on the atomic distribution within the crystal lattice. A unit cell is the smallest part of a crystal lattice that demonstrates the three-dimensional pattern of the entire crystal, representing the minimum volume repeated throughout the solid. In a three-dimensional space, all lattices can be classified into seven crystal systems (Bravais lattices) based on the relative lengths and angles of their axes or their respective symmetries. As a result, each X-ray diffraction pattern provides a unique "fingerprint" of the periodic atomic arrangement of the material analyzed, which is the unit cell crystal system and the lattice parameters.
Polymorphism, where molecules or atoms are arranged in different ways in a crystalline solid, results in different diffraction patterns for each polymorph. Each polymorph's X-ray diffraction pattern is distinct and serves as its unique identifier. From XRD it's also possible to infer the relative stability of polymorphs, by confronting the calculated specific volume of each phase [46] (by applying the density rule proposed by Burger, see Section 2.3).

3.2.1. Experimental setup

The process begins with X-rays being emitted from a Cu cathode in an X-ray tube. After passing through a Ge monochromator, the X-ray beam (with a wavelength $\lambda = 1.54056$ Å) is filtered and collimated before being directed toward the sample. The sample, in powder form, is placed in a 0,5 mm diameter glass capillary at the center of a sample holder. The diffracted X-ray intensity is collected by a CPS-120 detector, allowing for simultaneous data collection in an angular range between 4° and 120°. Measurements as a function of temperature were carried out using a liquid nitrogen 700 series Cryostream Cooler from Oxford Cryosystems. Before each isothermal data acquisition, the specimen was allowed to equilibrate for about 10 min, and each acquisition time was no less than 1 h.

4. Experimental part and discussion of results

4.1. Presentation of the compound

Orcinol (IUPAC name: 5-methylbenzene-1,3-diol) is a phenolic organic compound, with brute formula $CH_3C_6H_3(OH)_2$. It is found in nature in several species of lichens like *Roccella tinctoria*. At room temperature it presents itself as a colorless solid that becomes red by air exposure. Its chemical structure closely resembles that of resorcinol with an added methyl group instead of a hydrogen atom. Orcinol forms a hydrate with water, orcinol monohydrate. It has been shown that it easily forms an array of co-crystals with many different organic compounds [49,50,51], among which orcinol glucoside stands out for therapeutic reasons (both as an antidepressant[16,17] and osteogenesis factor[18]). It was also shown that, when subjected to oxidative polymerization using different oxidants such as NaOCl, H_2O_2, and air between 50 and 90 °C, oligopolymers of different chain length (oligo(orcinol)) could be formed [47], and was even utilized as a monomer for a bio-degradable polyester[48].

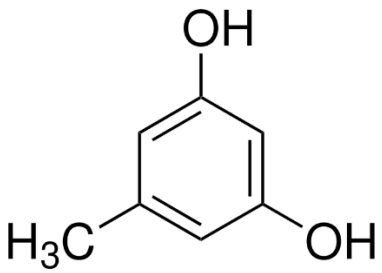

***Figure 4.1**. Orcinol molecule*

Orcinol molecule shows conformational isomerism, as both hydroxyl groups are free to rotate on the C-O bond. Among all conformations that orcinol can assume, three are the most stable (lowest energy): *syn–syn*, *anti–anti* and *syn–anti*. The difference is related to the orientation of the OH groups benzene plane, as shown in Figure 4.2(a). In Figure 4.2(b) is presented the relaxed linear potential energy scan for OH group rotation, showing low interconversion barrier between them (calculated by Mukherjee et al.[51]).

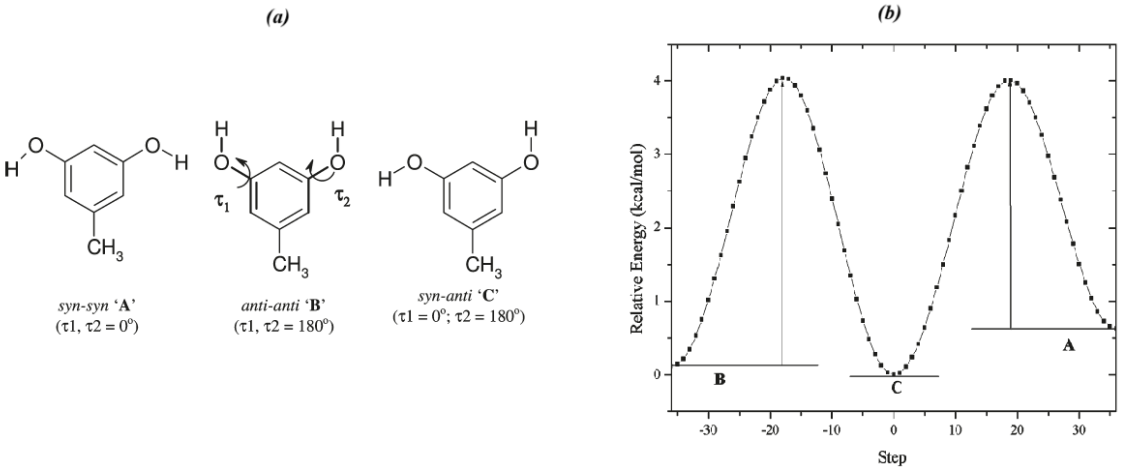

***Figure 4.2**. Conformational isomers of orcinol (**a**); relaxed linear potential energy scan for OH group rotation (**b**)* [51]

It's a well-established fact that the existence of conformational isomers, for a given molecule, can result in several polymorphs. In a previous work, Mukherjee *et al.* determined the crystal structure of two polymorphs, a pseudopolymorph and several co-crystals of orcinol [51]. Solid orcinol was obtained by crystal growth from different solutions. From a $CHCl_3$ solution, an anhydrous Form I was obtained, while from a nitromethane solution a second anhydrous Form II was obtained. It was reported that most of the attempts resulted in the formation of orcinol monohydrate, the hydrate form of orcinol, thus being classified as its pseudopolymorph. Single crystal X-ray diffraction was also performed at 150 K on the different polymorphs. Form I showed tetragonal structure, both symmetry independent molecules (Fig. 4.2(a)) adopt the *syn–anti* conformation. Form II had orthorhombic structure characterized by a one-dimensional chain of O−H· · ·O hydrogen bonds consisting of a sequence of four symmetry independent molecules in the order *syn–syn*, *anti–anti*, *syn–anti* and *syn–anti* [52] (Fig. 4.2(c)). For Form I and II, lattice parameter values are reported in Section 4.4 in Table 4.2. In Figure 6.4 are reported visual representations of molecular arrangements of Form I, Form II and orcinol monohydrate.

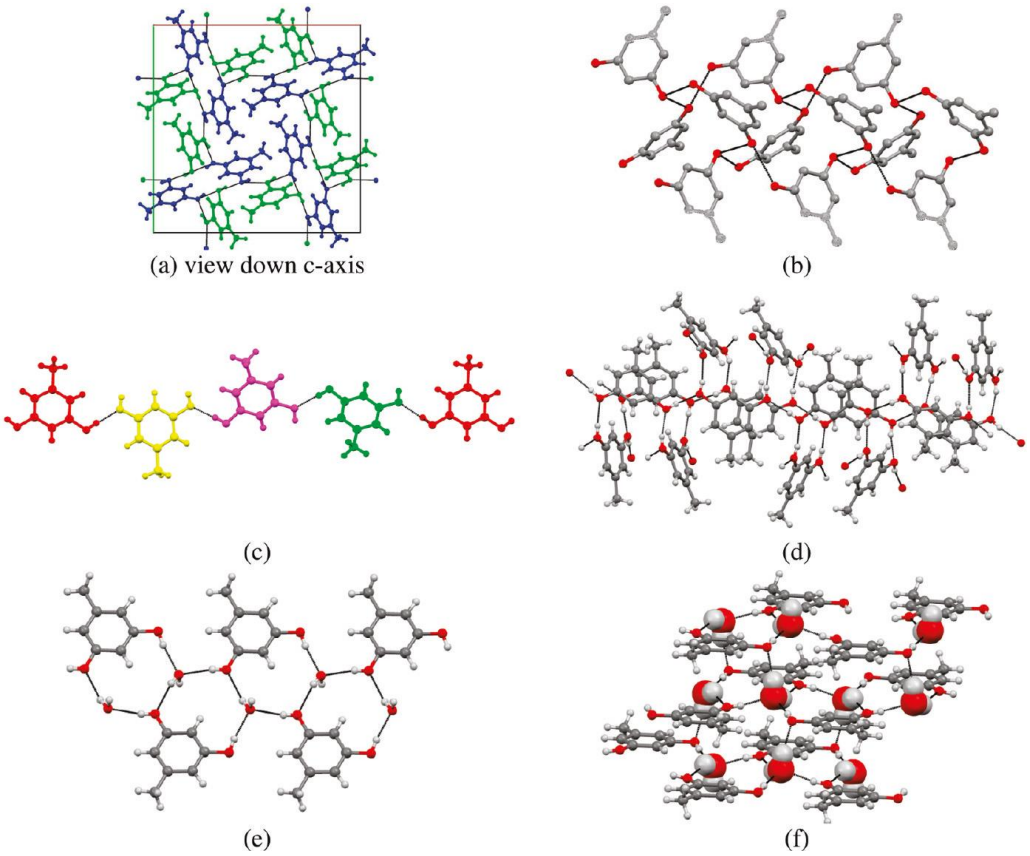

***Figure 4.4**. Crystal packing representation of Form I (a-b), Form II (c-d) and orcinol monohydrate (e-f)* [50]

Form I shows tetragonal structure, while Form II has orthorhombic structure. At 150 K, Form I (ρ = 1,276 g/cm^3) is denser than Form II (ρ =1,205 g/cm^3). Then Form I can be considered more stable than Form II, by the density rule proposed by Ramburger (see Section 2.3).

Regarding thermal proprieties of orcinol, one study by Mozaffari *et al.* measured at normal pressure its melting temperature T_m [53]. The value reported was T_m = 109 ± 0,23 °C. In another work [54], Kirithivasan found a similar value for T_m as the one of Mozaffari (T_m = 109,61 °C) along with the corresponding melting enthalpy of ΔH_m = 145,1 J/g.

4.2. Purification of analyzed powder

It's well established that orcinol forms a hydrate crystalline structure with water, denoted as orcinol monohydrate. Previous works [55] show that orcinol favorably combines with water to form its hydrate. Thus, two-step preliminary experiments were done to determine if the data to be collected could correctly be attributed to pure orcinol in crystalline form, or to orcinol monohydrate (or some other potential co-crystals that could heterogeneously nucleate from impurities).

Firstly, thermal analyses (TGA and DSC) were conducted to characterize thermally both orcinol monohydrate and orcinol Thermofischer 98%. DSC graphs of both are shown in overlay in Figure 4.5. Powder samples of the two compounds were heated from 20 °C to above 120 °C with a heating rate of 2 °C/min.

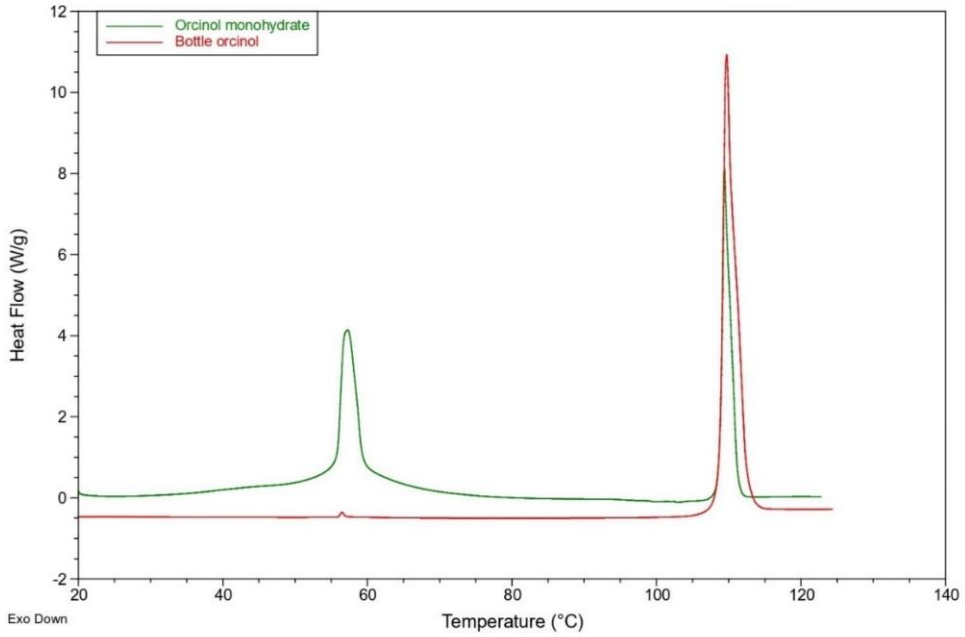

***Figure 4.5**. Comparison between DSC scans of bottle orcinol (in red) and orcinol monohydrate (in green)*

DSC scans of orcinol monohydrate showed an endothermic peak around 56 °C (ΔH_m = 200 J/g) which belongs to the decomposition of the monohydrate in water plus orcinol [56]. The second peak at around 110 ºC corresponds to the melting of orcinol. Thus, for orcinol Thermofischer 98%, the appearance of the small peak at 56 ºC shows that the hydrate is present in this product.

Results of TGA showed that a significant weight loss was detected after 60 °C in orcinol monohydrate, as in Figure 4.6. The weight loss detected was attributed to water escaping after dissociation in its vapour state. However, TGA of orcinol Thermofischer 98% don't show any detectable loss at 60 ºC and only at around 150 ºC a weight loss is detected.

Finally, samples of orcinol Thermofischer 98% and orcinol monohydrate were analyzed by X-ray diffraction. Although both patterns are different, the position of some of the most intense peaks (which characterize the spectrum) of the two samples coincided. For this reason, it was impossible to determine with this experimental technique if orcinol Thermofischer 98% was contaminated by its monohydrate.

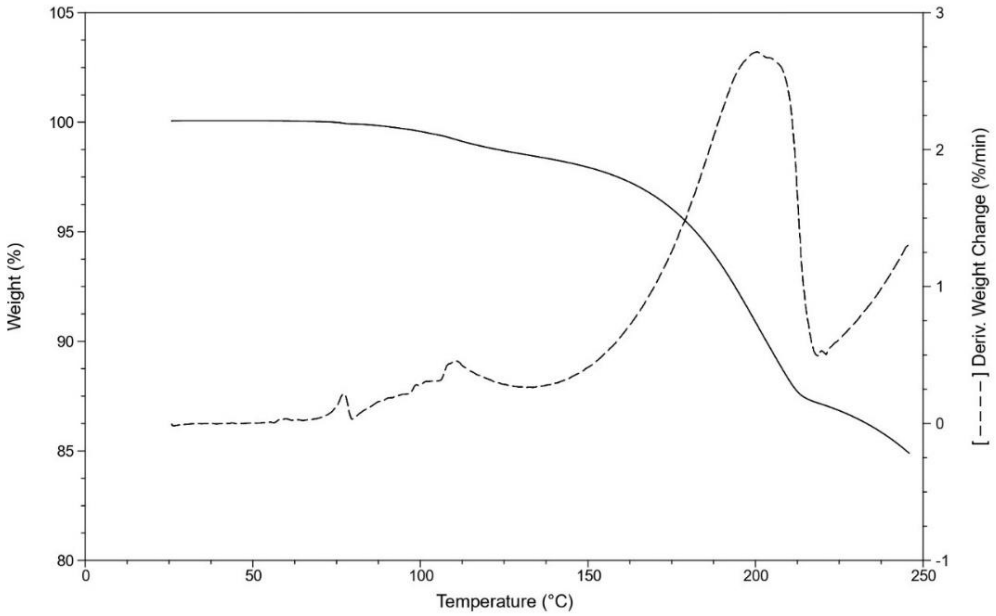

***Figure 4.6**. TG curve (continuous line) and its time derivative (DTG curve) (dotted line) of orcinol monohydrate, highlighting the weight loss occurring after 60 ºC*

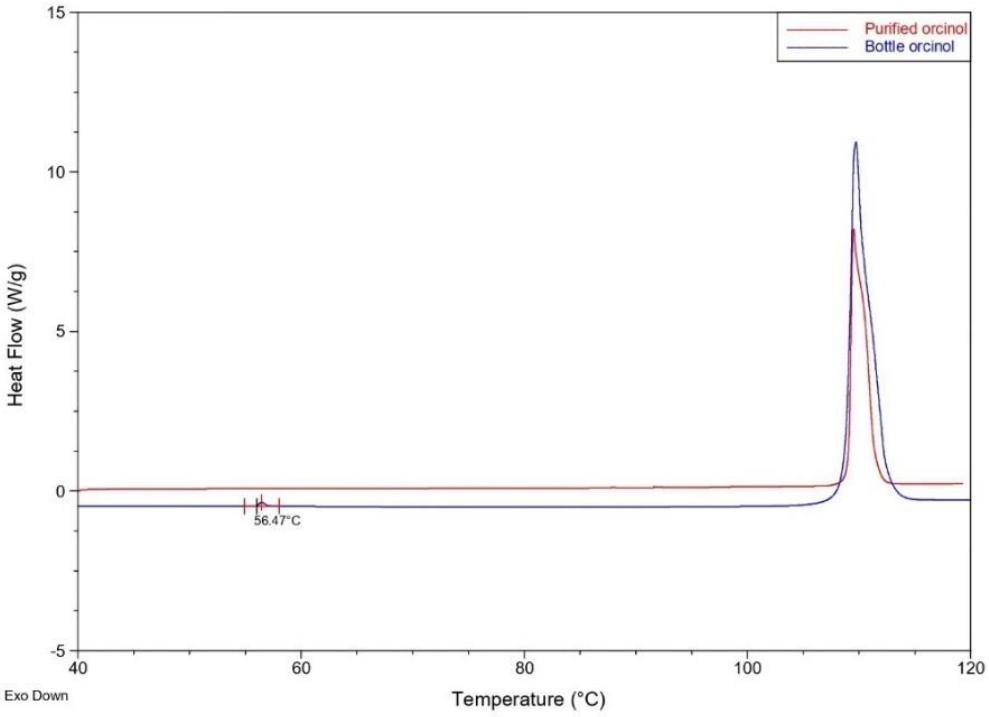

***Figure 4.3**. Comparison of DSC scans of orcinol Thermofischer 98% before purification (in blue) and after (in red)*

Thus, to eliminate the water content of the orcinol, a purifying procedure was devised and subsequently applied to all orcinol samples utilized in this study, such as in DSC at ambient pressure, DTA at high pressure and XRD.
The drying procedure consisted in putting bottle orcinol in a crystallizer on a heating plate at 60 °C for at least an hour. The product obtained was dehydrated orcinol (hereby denoted as "purified orcinol") from the DSC and TGA measurements. The DSC scan of purified orcinol can be seen in Figure 6.7 where the signal at 56ºC has disappeared.
Figure 4.8 shows a comparison between TGA runs of orcinol monohydrate and purified orcinol. The loss of water present in the monohydrate is not present in purified orcinol.

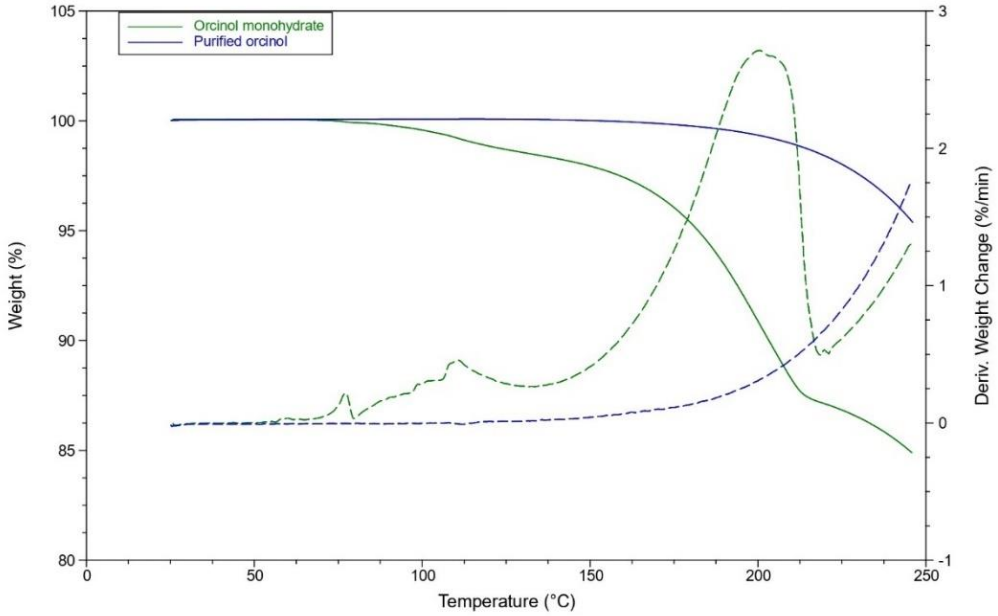

***Figure 4.4**. Comparison between TG plots of purified orcinol (in blue) and orcinol monohydrate (in green)*

The purified sample was analyzed by XR to determine if it corresponded to some of the polymorphs found in literature. In Figure 4.9, the experimental pattern for the purified sample is compared with the theoretical pattern of the tetragonal structure of one of the anhydrous polymorphs found by Mujahedee *et al*.[51], namely Form I. Then, it was concluded that the purified sample is Form I.

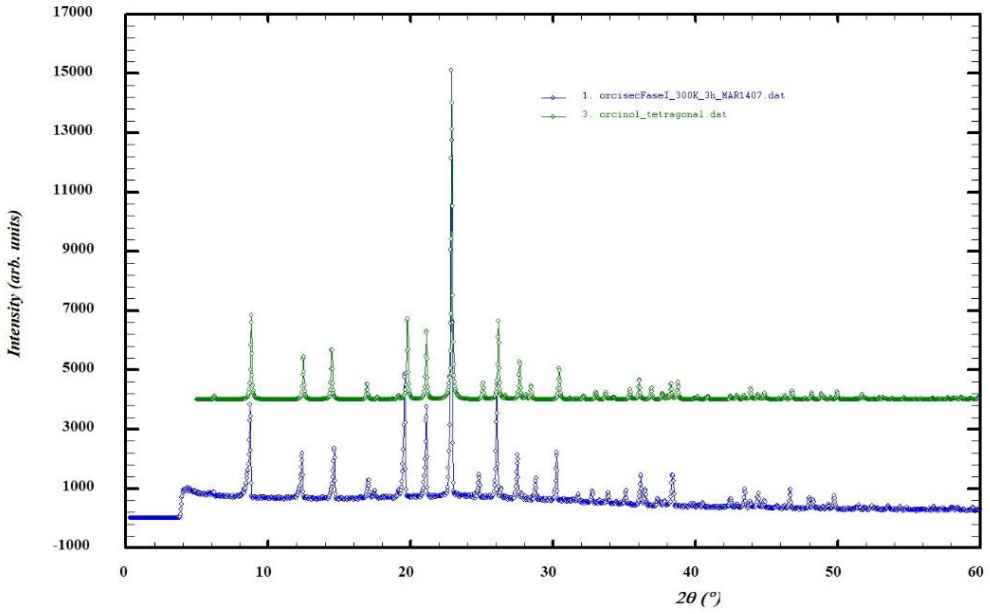

***Figure 4.5**. XR spectra of purified orcinol (in blue) and Form I (in green)*

4.3. DSC at normal pressure

After having performed the purification procedure explained in the previous section, heat-flux DSC scans at ambient pressure were done to determine thermodynamic properties of orcinol, such as its melting temperature T_m and enthalpy of fusion ΔH_m, as well to investigate the formation of its metastable forms.

DSC scans were designed as follows:

1. first heating from 20 °C to 125 °C
2. first cooling from 125 °C to -50 °C (or -70 °C)
3. second heating run from -50 °C (or -70 °C) to 125 °C.

Heating and cooling rates were held constant during a single DSC run, but varied across different measurements. Temperature change rates were set at

a) 2 °C/min
b) 5 °C/min
c) 10 °C/min

This was done in order to investigate the dependence of the measured properties at different heating and cooling runs.

In the first heating ramp (20 °C to 125 °C), a sharp endothermic peak was always observed at around 109 °C, regardless of the heating rate, as shown in Figure 4.10.

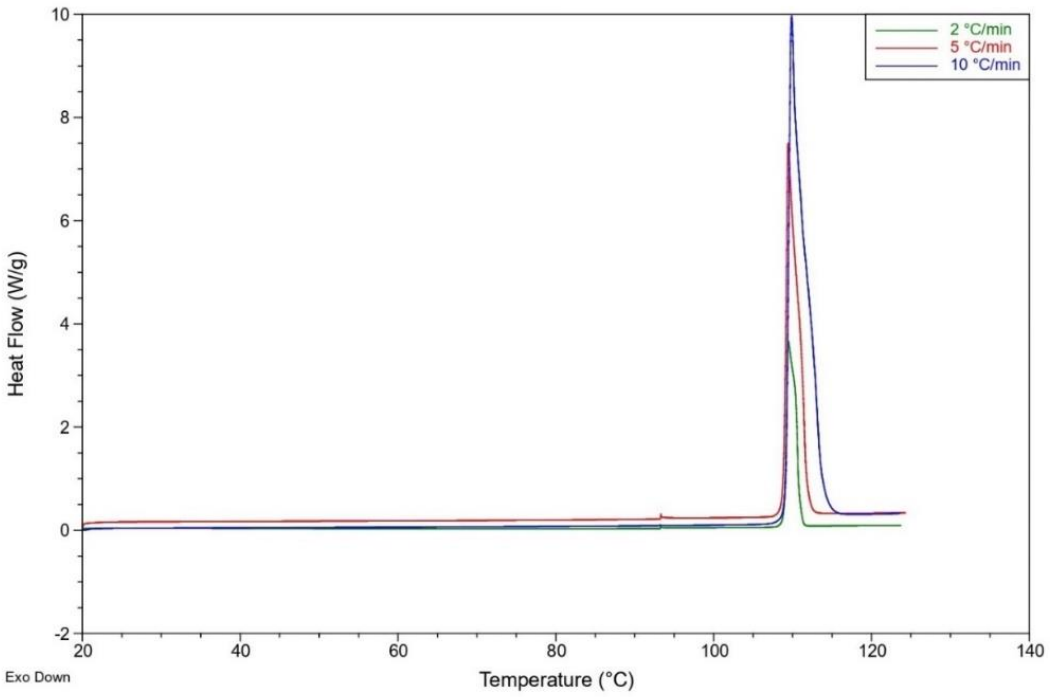

***Figure 4.6**. DSC plots at heating rates of 2 °C/min (in green), 5 °C/min (in red) and 10 °C/min (in blue) all showing a peak at 109 °C*

This peak was associated with the phase transition of orcinol from its stable phase (denoted as phase I) at room temperature and pressure to its liquid phase, hereby denoted as I→L.

From the measurements both melting temperature and melting enthalpy were extracted. The average values were found to be

- $T_{m,I}$ = 108,87 °C (383,12 K)
- $\Delta H_{m,I}$ = 162,61 J/g

Melting temperature agrees with data reported by Maraffaza *et al*.[53] and Kirithivasan[54]; however the value of melting enthalpy as here measured is 10% greater than the one reported by Kirithivasan.

During the cooling ramp, exothermic peaks of different shapes were recorded. However, these peaks were not analyzed. In some instances of high heating and cooling rates (10 °C/min), the exothermic peaks were recorded during the second heating ramp, but showed a similar shape nevertheless.

During the second heating ramp two different endothermic peaks were detected. Both of them appeared alone (no other endothermic peak was recorded in the same heating ramp).

In most cases, a single endothermic peak was found at circa 84 °C is shown in Figure 4.12. This peak was attributed to the phase transition of another solid phase of orcinol (hereby denoted as phase III) into liquid, transition III→L. This phase appears to be metastable at room temperature and pressure. The average values of the melting temperature and enthalpy were found to be

- T_m = 84,24 °C (358,39 K)
- ΔH_m = 116,01 J/g

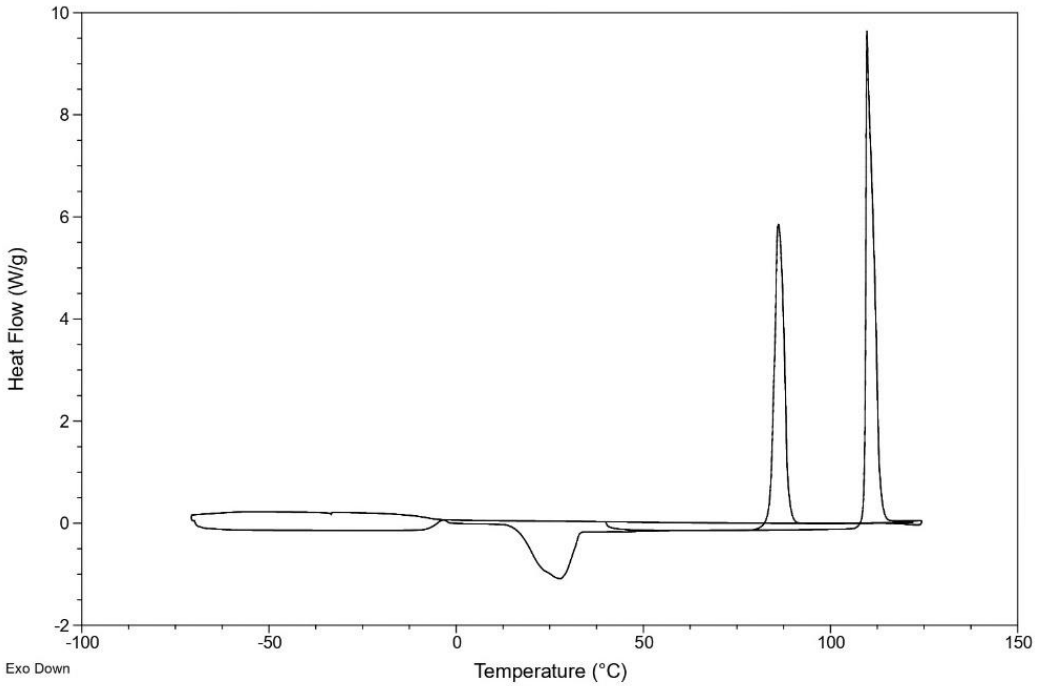

***Figure 4.12**. DSC thermogram showing the behavior of one sample: 1st heating, endothermic peak at 110 °C; 1st cooling without signals; 2nd heating, glass transition at -5ºC, exothermic peak at around 25-30 °C and endothermic peak at 84 °C.*

However, this peak was not the only one found in the second heating run of all orcinol samples. In a small minority of cases, another single endothermic peak appeared at 97 °C. An example of a DSC run with this behavior is shown in Figure 4.13. It occurred in measurements conducted with a higher cooling rate (of 10 °C/min). This peak was hypothesized belonging to another metastable phase of orcinol (hereby denoted as phase II) into liquid, transition II→L. The average values of melting temperature and enthalpy, for this phase, are

- T_m = 97,06 °C (371,21 K)
- ΔH_m = 149,55 J/g

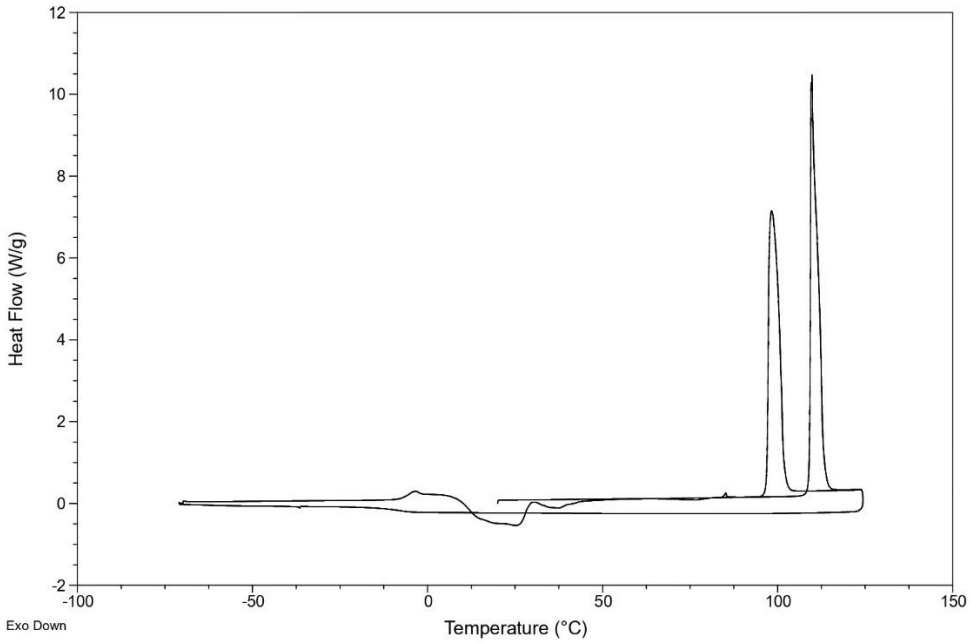

***Figure 4.13**. DSC thermogram showing the behavior of a sample: 1st heating, endothermic single peat at an endothermic peak at 110 °C; 1st cooling without signals; 2nd heating, glass transition at -5 °C, exothermic peak at around 25-30 °C and endothermic peak at 97 °C.*

It was also found that, in the runs with temperature change rate of 10 °C/min, all resulting thermograms showed an inflection point at -5 °C, Figure 4.14. This was interpreted as the glass transition point of orcinol, showing that orcinol could also be found in an amorphous state. However, further characterization of the glass state of orcinol was out of the scope of this work.

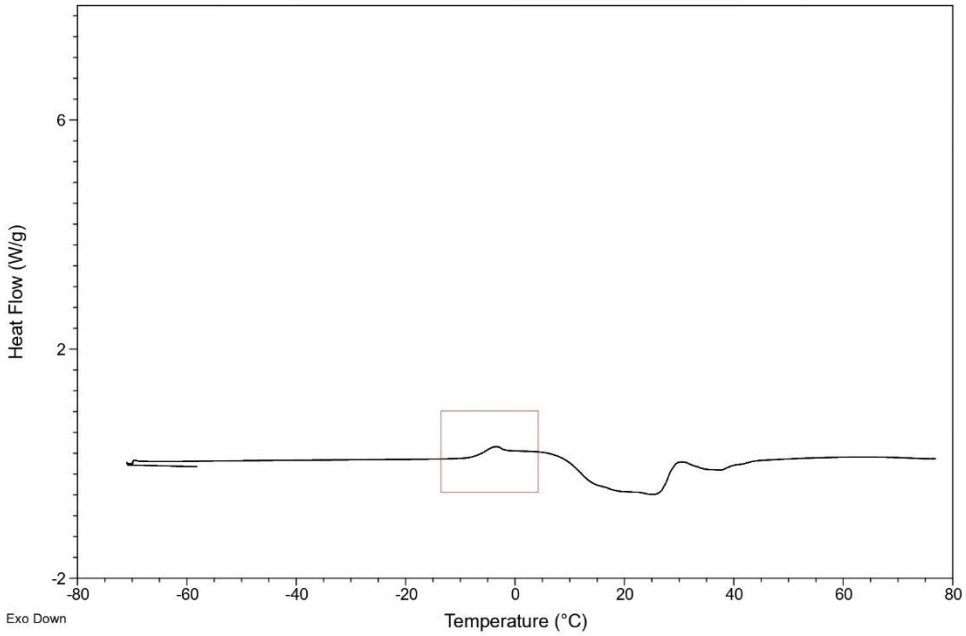

***Figure 4.14**. DSC thermogram showing a glass transition point (in the gray box)*

Based on DSC measurements, we can conclude that the compound has three different polymorphs with different melting temperatures and enthalpies. Based on these temperatures, the phase I has been named as the one with the highest melting point, and the remaining phases in descending order of melting temperatures. According to the stability criteria, phase I would be the stable phase, phase II the metastable phase, and phase III the supermetastable phase. Table 4.1 summarizes the data presented in this section.

***Table 4.1**. Average values and standard deviations of melting temperatures and enthalpies for the three phases detected*

State transition	T *(K)*	ΔH *(J/g)*
I→L	382,01 ± 0,28	162,61 ± 3,04
II→L	370,20 ± 0,07	149,55 ± 3,81
III→L	357,38 ± 0,17	116,01 ± 3,00

4.4. Arguments for determining the relationship between polymorphs. Calculation of transition temperatures T_{I-II}, T_{I-III} and T_{II-III}

Following Burger and Ramburger's criteria that they proposed (as discussed in Section 2.3), calculations were done in order to determine how each polymorph is related to one another at normal pressure. In particular, the criteria here adopted were two. The first was the *heat-of-fusion* rule, that

states that in an enantiotropic system the higher melting polymorph will have the lower heat of fusion. If the higher melting polymorph has a higher heat of fusion the two are related monotropically. Then, it can be concluded that the three trimorphs are monotropically related to one another at normal pressure, as

$$\Delta H_{m,I} = 162{,}61\ \frac{J}{g} > \Delta H_{m,II} = 149{,}55\ \frac{J}{g} > \Delta H_{m,III} = 116{,}01\ \frac{J}{g} \qquad \text{Eq. 4.1}$$

However, as Burger and Ramburger have pointed out, when melting points aren't close ($\Delta T \approx 30$ K) this rule might not work. As this was the case, a second rule was followed to confirm the results.

The second one was the *entropy-of-fusion* rule. According to this rule, if the polymorph with the higher melting point has the lower entropy of fusion, the two modifications are enantiotropically related. If the lower melting form has the lower entropy of fusion, then the two forms are monotropically related. Entropy of fusion is calculated as

$$\Delta S_m = \frac{\Delta H_m}{T_m} \qquad \text{Eq. 4.2}$$

Where ΔH_m is the melting enthalpy and T_m is the melting temperature. If the peaks recorded by DSC were correctly attributed to, then,

$$\Delta S_{m,I} = \frac{\Delta H_{m,I}}{T_{m,I}} = \frac{162{,}61\ \text{J/g}}{382{,}01\ K} = 0{,}426\,\frac{J}{g\ K} \qquad \text{Eq. 4.3a}$$

$$\Delta S_{m,II} = \frac{\Delta H_{m,II}}{T_{m,II}} = \frac{149{,}55\ \text{J/g}}{370{,}2\ K} = 0{,}404\,\frac{J}{g\ K} \qquad \text{Eq. 4.4b}$$

$$\Delta S_{m,III} = \frac{\Delta H_{m,III}}{T_{m,III}} = \frac{116{,}01\ \text{J/g}}{357{,}38\ K} = 0{,}325\,\frac{J}{g\ K} \qquad \text{Eq. 4.5c}$$

And since $\Delta S_{m,I} > \Delta S_{m,II} > \Delta S_{m,III}$ it was again concluded that the three polymorphs are monotropically related at normal pressure.
Moreover, the transition temperatures between polymorphs $T_{I\text{-}II}$, $T_{I\text{-}III}$ and $T_{II\text{-}III}$ at normal pressure were calculated by utilizing the data collected by DSC.
The theoretical reasoning is as follows. Taking into account a system comprised of phase I and II (a system undergoing transition I-II, for example) at constant pressure, the equilibrium condition $dG = 0$ implies that, in that point, $G_I = G_{II}$. Assuming that the capacity contribution in the range of temperatures considered is negligible, Gibbs energy variation can be expressed as:

$$\Delta G_{I-II} = \Delta H_{I-II} - T\Delta S_{I-II} \qquad \text{Eq. 4.6}$$

Since both enthalpy and entropy are state functions, the right side of Eq. 4.6 can be reformulated considering that

$$\Delta H_{I-II} = (H_L - H_{II}) - (H_L - H_I) = \Delta H_{m,II} - \Delta H_{m,I} \qquad \text{Eq. 4.7}$$

$$\Delta S_{I-II} = (S_L - S_{II}) - (S_L - S_I) = \Delta S_{m,II} - \Delta S_{m,I} \qquad \text{Eq. 4.8}$$

By combining Eq. 4.2, 4.7 and 4.8:

$$T_{I-II} = \frac{\Delta H_{I-II}}{\Delta S_{I-II}} = \frac{\Delta H_{m,II} - \Delta H_{m,I}}{\Delta S_{m,II} - \Delta S_{m,I}} \qquad \text{Eq. 4.9}$$

The same reasoning is valid for transitions I-III and II-III. The values of the transition temperatures at normal pressure are thus calculated as follows:

$$T_{I-II} = \frac{\Delta H_{m,II} - \Delta H_{m,I}}{\Delta S_{m,II} - \Delta S_{m,I}} = \frac{(149{,}55 - 162{,}61)\ \text{J/g}}{(0{,}404 - 0{,}426)\ \text{J/g K}} = 593{,}64\ K = 320{,}5\ ℃ \qquad \text{Eq. 4.10a}$$

$$T_{I-III} = \frac{\Delta H_{m,III} - \Delta H_{m,I}}{\Delta S_{m,III} - \Delta S_{m,I}} = \frac{(116{,}01 - 162{,}61)\ \mathrm{J/g}}{(0{,}325 - 0{,}426)\ \mathrm{J/g\ K}} = 461{,}39\ K = 188{,}25\ ℃ \qquad \text{Eq 4.10b}$$

$$T_{II-III} = \frac{\Delta H_{m,III} - \Delta H_{m,II}}{\Delta S_{m,III} - \Delta S_{m,II}} = \frac{(116{,}01 - 149{,}55)\ \mathrm{J/g}}{(0{,}325 - 0{,}404)\ \mathrm{J/g\ K}} = 424{,}56\ K = 151{,}41\ ℃ \qquad \text{Eq 4.10c}$$

All the transition temperatures take place at temperatures higher than the respective melting points, i.e. at temperatures where the stable phase is the liquid phase. This fact is characteristic of a monotropic behavior.

In Figure 4.15 is shown a proposed qualitative *G(T)* plot of the phases here found, with reported melting and transition temperatures.

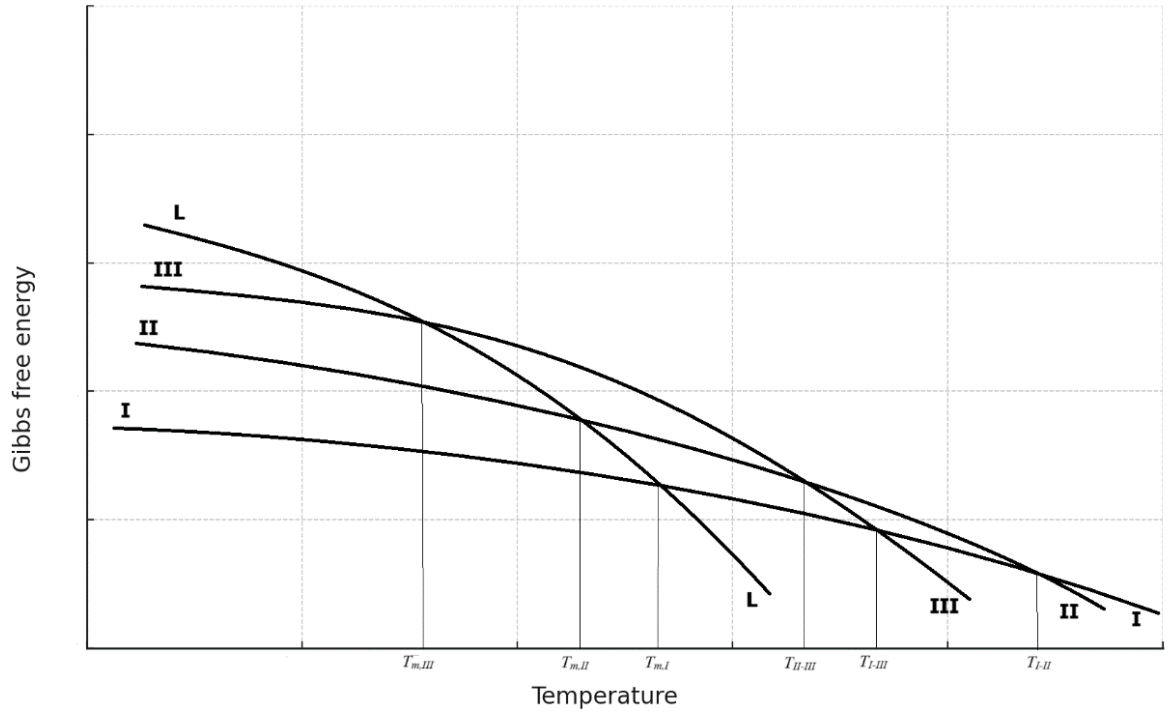

***Figure 4.15**. Qualitative G(T) plot of the various phases involved*

After this, X-ray diffraction analyses were done to determine the crystalline lattice of the phases here found.

4.5. X-ray diffractometry

As discussed in Section 4.1, previous XRD analysis [57,58] conducted on solid orcinol at 150 K showed that orcinol could form (at least) two different crystalline structures, one with a tetragonal unit cell while the other with an orthorhombic one. The corresponding lattice parameters for the two polymorphs are summarized in Table 4.2. Theoretical patterns derived from the structural published structures (CCDC) are shown in Figure 4.16 and visual representation of the unit cells is given in Figure 4.17 and 4.18.

***Table 4.2**. Lattice parameters for polymorphs I and II at 150 K [57,58]*

Polymorph	*Space group*	*a*	*b*	*c*	*V*	*Z*
Form I	Tetragonal I-4	20.060(3)	20.060(3)	6.4230(13)	2584.6(8)	16
Form II	Orthorhombic $P2_12_12_1$	13.784(14)	16.174(17)	24.55(2)	5473(9)	32

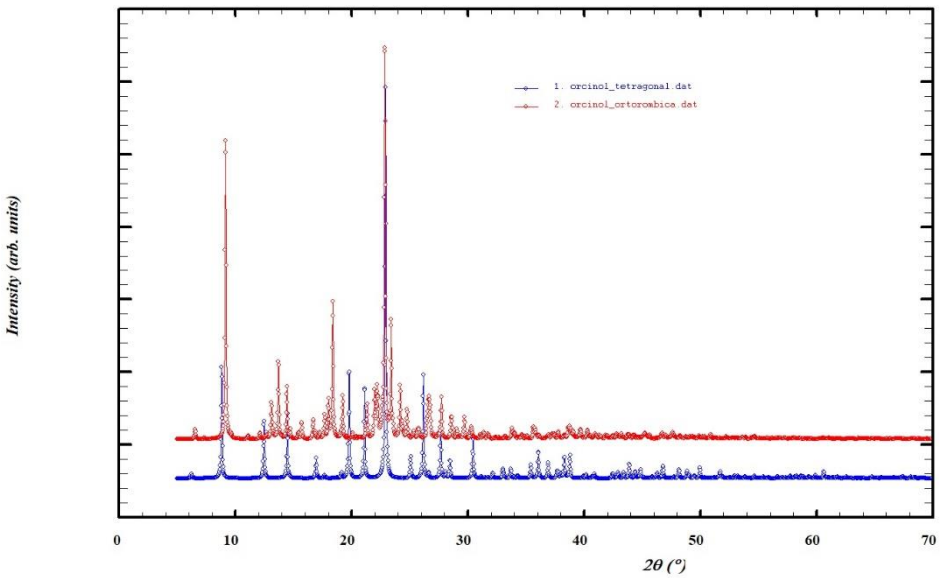

***Figure 4.16**. XR patterns at 150 K for polymorph I (in blue) and polymorph II (in red) as per CCDC data [57,58]*

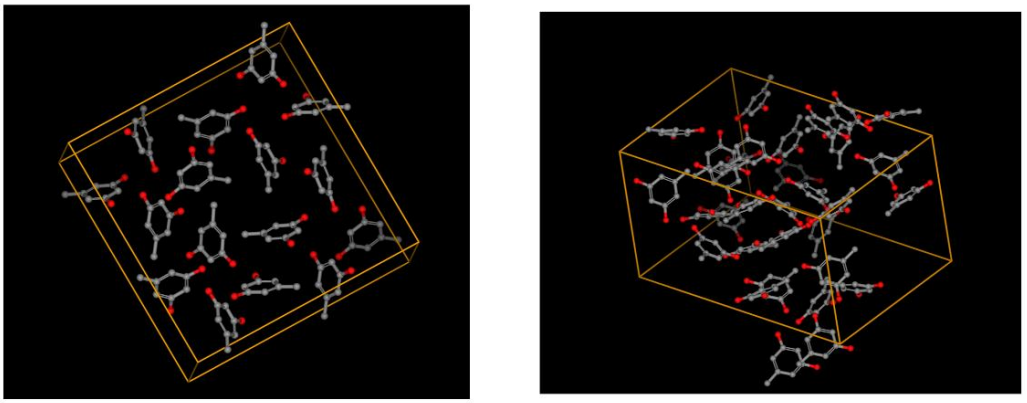

***Figure 4.17**. Visual representation of the disposition of orcinol molecules in (**a**) tetragonal and (**b**) orthorhombic system*[57,58]

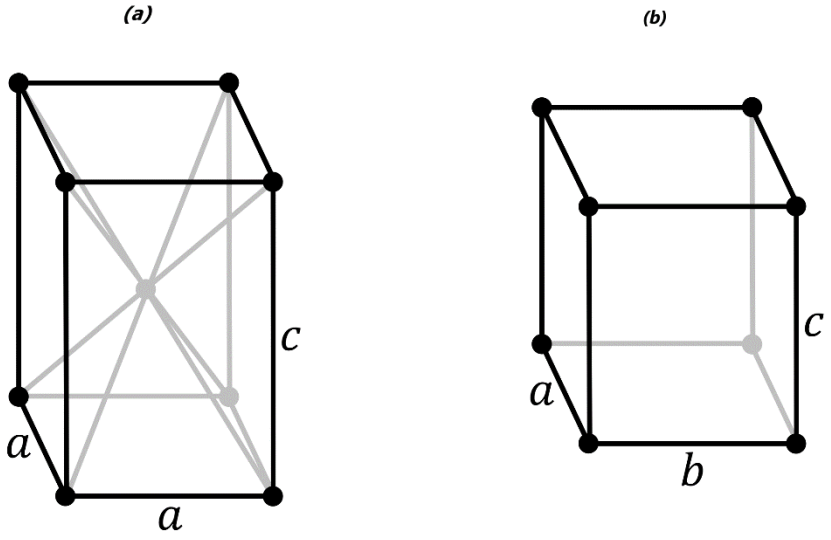

***Figure 4.18**. Representation of the Bravais lattice of (**a**) body centered tetragonal and (**b**) primitive orthorhombic*

From the CCDC data it was possible to obtain the XR pattern at the operating conditions of the diffractometer that was used in the following measurements (in particular the X-ray wavelengths changes as CCDC data is from single crystal XRD utilizing Mo-Kα, while in this work by powder XRD utilizing λ Cu).

Assuming that at room temperature the spectrum of the purified sample is the same one that was obtained at 150 K (Form I) and the results of the DSC (that show only one endothermic signal of the melting is obtained in the first heating), it must be concluded that any

transformation between Form I and the other phases has to occur between 150 K and the melting point of Form I. This hypothesis has been verified through XRD.
As presented in Figure 4.9, the spectrum of purified orcinol mostly coincides with the spectrum of Form I. From this it's possible to conclude that the experimental spectrum can be indexed by means of the lattice and spatial group of the tetragonal form. This indexing procedure is called Pattern Matching or Le Bail adjustment and it's included in the software utilized to analyze the spectra, FullProof program[59]. By means of this procedure, the lattice parameters (that are changing with temperature because of thermal expansion) were obtained at every measured temperature. In Figure 4.18 the result of the adjustment for the measurement at 300 K is shown. Only peaks corresponding to the special group considered are present in the experimental pattern. The refined parameters are shown in Table 4.3.

***Table 4.3**. Lattice parameters of Form I at 300 K*

T (K)	*Spacegroup*	*a (Å)*	*b (Å)*	*c (Å)*	*V (Å^3)*
300	82	20.293(1)	20.293(1)	6.3494(5)	2614.8(3)

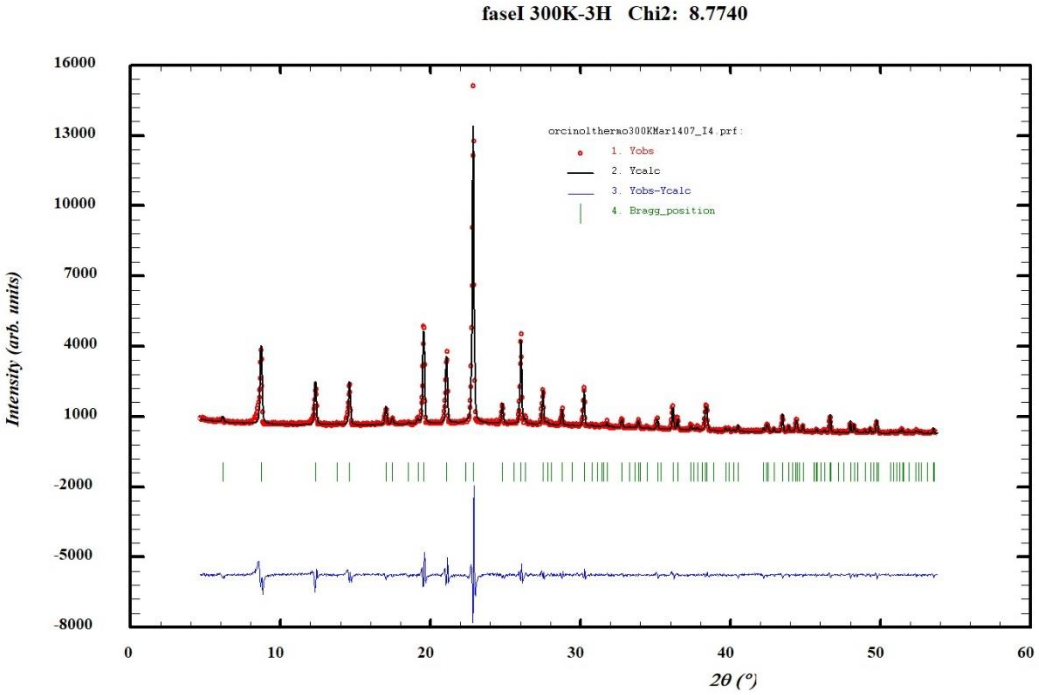

***Figure 4.19**. Experimental (red) and refined (black) diffraction patterns along with difference profile(blue) and Bragg reflections of the tetragonal form at 300 K (green bars)*

The spectra of the purified sample were measured between 160 K and its melting point (383 K) at several temperatures with acquisitions times of 1 hour and are represented in Figure 4.20. The results of the pattern matching adjustment are included in Table 4.4. The evolution of the parameters as a

function of temperature are shown in Figures 4.21, 4.22 and 4.23. Parameter *a* increases with temperature, while parameter *c* decreases. However, unit cell volume increases with temperature, as expected.

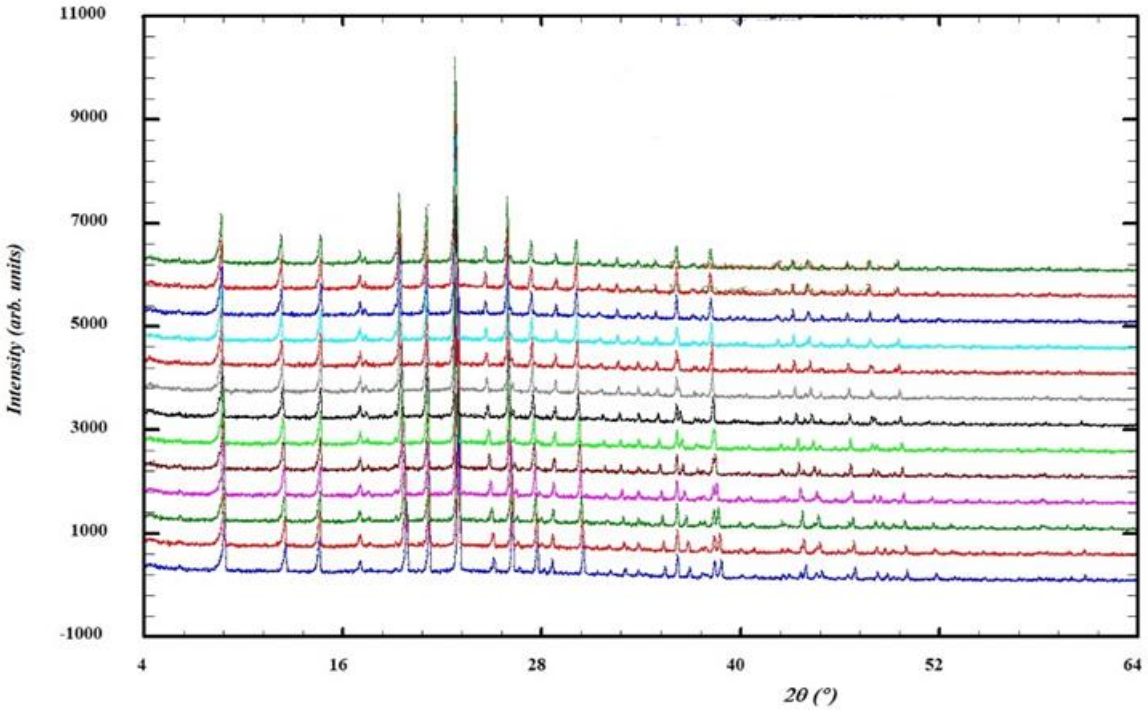

***Figure 4.20**. Experimental patterns at 160 K, 190 K, 220 K, 250 K, 280 K, 300 K, 320 K, 340 K, 350 K, 360 K, 370 K, 375 K and 380 K (From bottom to top) for Form I*

***Table 4.4**. Lattice parameters of Form I at different temperatures*

Temperature (K)	*a (Å)*	*c (Å)*	*V (Å^3)*
160	20.046(1)	6.3889(6)	2567.3(3)
190	20.097(1)	6.3802(5)	2576.9(3)
220	20.152(1)	6.3723(5)	2587.9(3)
250	20.203(1)	6.3627(6)	2597.1(3)
280	20.259(1)	6.3543(5)	2607.9(3)
300	20.293(1)	6.3494(5)	2614.8(3)
320	20.337(1)	6.3425(5)	2623.2(3)
340	20.381(2)	6.3375(6)	2632.5(4)
350	20.398(2)	6.3314(8)	2634.4(5)

360	20.421(1)	6.3282(6)	2639.0(4)
370	20.444(2)	6.3249(6)	2643.6(4)
375	20.454(2)	6.3243(6)	2645.8(4)
380	20.448(2)	6.3255(6)	2644.8(4)

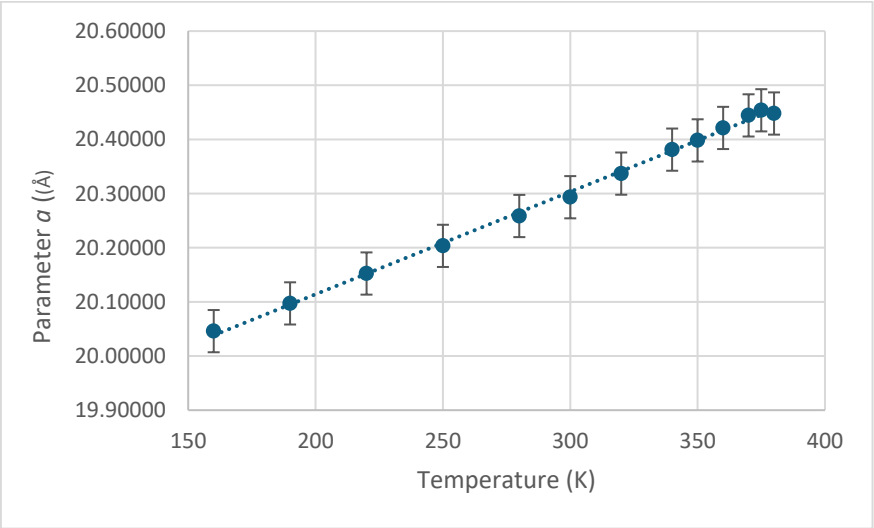

***Figure 4.21**. Evolution of parameter* **a** (Form I) *with temperature*

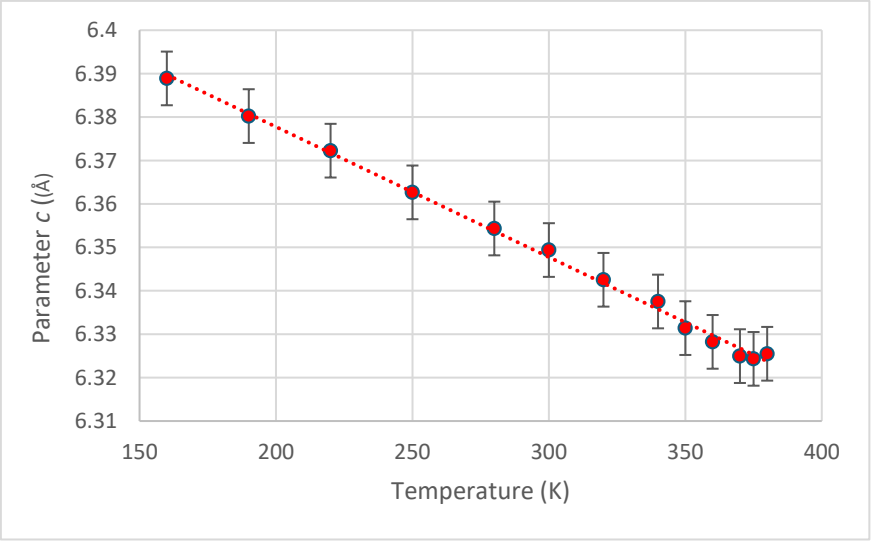

***Figure 4.22**. Evolution of parameter* **c** (Form I) *with temperature*

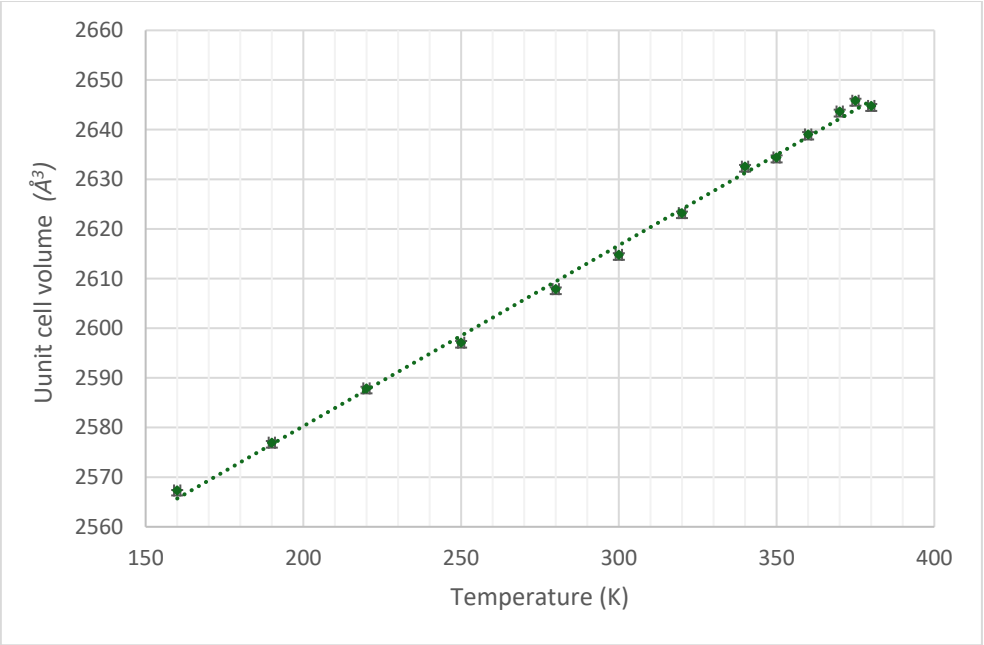

***Figure 4.23**. Evolution of unit cell volume (Form I) with temperature*

In DSC analyses, metastable phases were obtained from the crystallization of the liquid phase. A similar process was carried out in the diffraction measurements. The samples of dry orcinol that were identified as Form I (tetragonal structure) were melted and cooled at different rates in the capillary.

In most of the experiments performed, the liquid began to crystallize at temperatures between 273 K and room temperature (295-300 K). The most frequently obtained spectrum can be indexed with the lattice and space group of the orthorhombic phase obtained by Mukherjee *et al.*[51], although additional peaks not corresponding to this phase can be detected. Figure 4.24 shows one part of the indexed spectrum where this fact can be seen. The parameters values for the orthorhombic phase at 300 K are reported in Table 4.5.

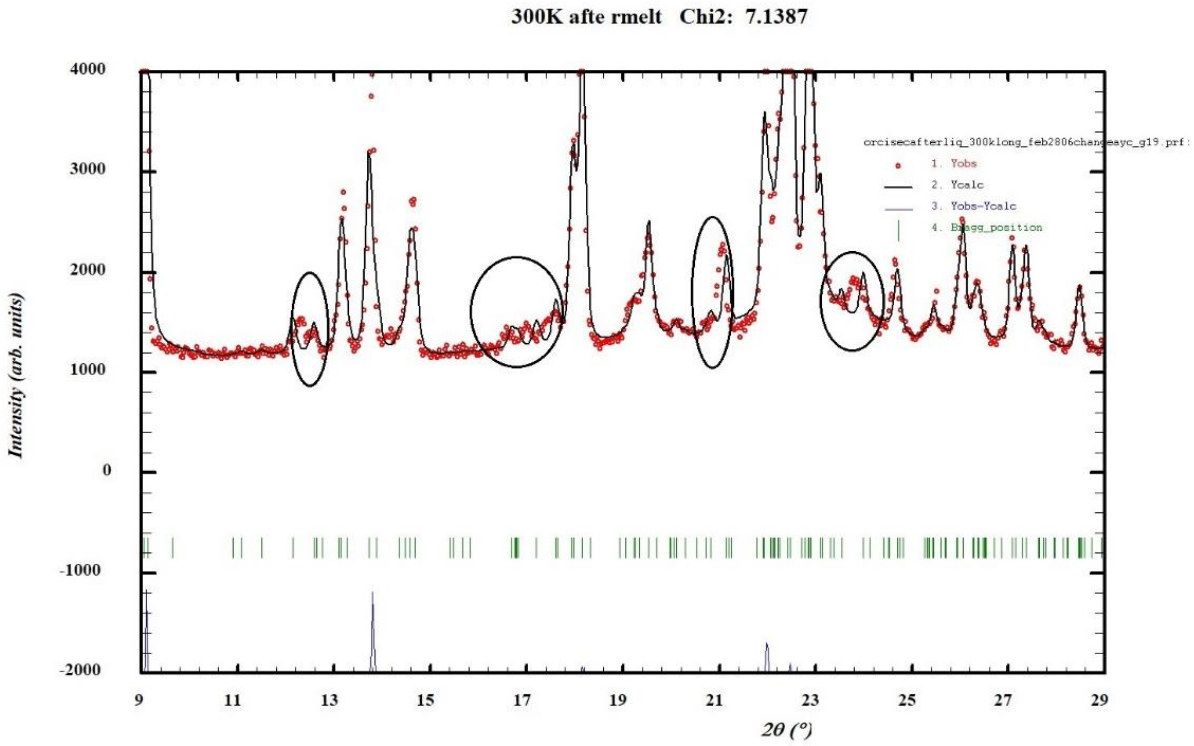

***Figure 4.24**. Partial spectrum (2ϑ: 9-29º) measured at 300 K of the sample crystallized from the liquid. Rounded circles indicate parts where the experimental pattern (red) does not match well the calculated orthorhombic (black).*

***Table 4.5**. Lattice parameters of the orthorhombic phase at 300K*

Temperature (K)	*a (Å)*	*b (Å)*	*c (Å)*	*V (Å³)*
300	24.5(4)	16.2(2)	13.8(2)	5492(1)

Regardless, the sample was cooled down to 150 K without detecting any change in the spectrum that could have indicated a transformation into another phase. Consequently, measurements were taken at increasing temperatures and all the measured spectra (150 K, 180 K, 210 K, 240 K, 270 K, 300 K) were indexed in the orthorhombic structure. The obtained volumes are represented in Figure 4.25 together with those obtained for the tetragonal phase. In the temperature range between 150 K and 300 K, these values show that the tetragonal phase is denser than the orthorhombic phase.

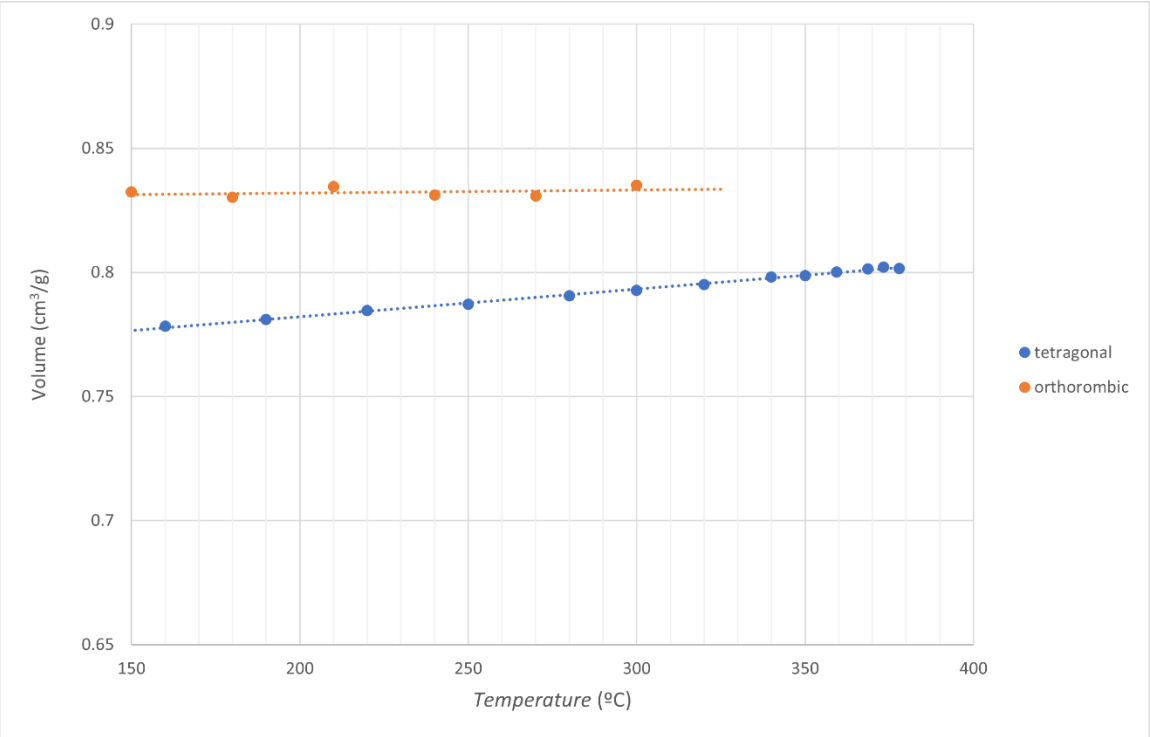

***Figure 4.25**. Volumes corresponding to the orthorhombic (orange) and tetragonal (blue) phases as a function of the temperature.*

In several cases, however, like heating of the orthorhombic phase at 340 K or maintenance at 300 K during night, changes can be observed in the spectra. In Figure 4.26 the orthorhombic phase measured at 300 K (pink) is shown together with the new spectra obtained at the same temperature 48 hours later (green) and the tetragonal form (brown) at the same temperature. Some peaks (marked by black thick line) could be related with the tetragonal form if it's assumed that this phase is most stable, but other peaks (marked by star) are newly arisen and do not correspond to the orthorhombic nor the tetragonal phase.

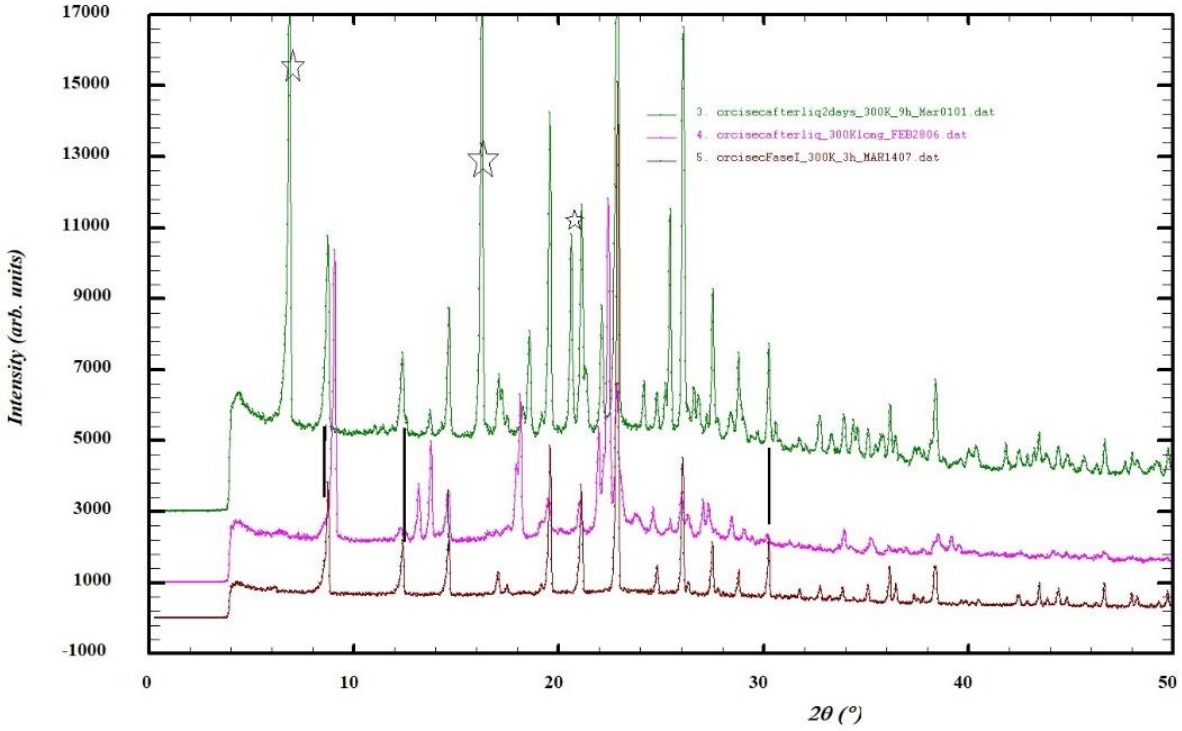

***Figure 4.26**. Experimental spectra at 300 K for the orthorhombic (pink) tetragonal (brown) phases together with the new evolution after 48h of the orthorhombic phase (green).*

From these last results it's concluded that it exists one new polymorph, hereby called I', more stable than the orthorhombic form (Form II). Its lattice parameters were not calculated.

Finally, one sample was cooled very quickly from the liquid phase to 273 K. The spectrum obtained at that temperature can be seen in Figure 4.27 (in blue). Subsequently, this sample was cooled until 150 K. Acquiring spectra at various temperatures yielded no observable changes in the spectrum. The sample was heated again to 273 K and maintained at this temperature all night. The spectrum obtained after this procedure is represented in Figure 4.27 (in green). This last spectrum is different from the previous one and resembles the one obtained from the orthorhombic phase, Form I'. However, the peaks that disappeared with time (marked by cross in the figure) must belong to another phase (Form I'') less stable than Form I'. Like in the case of Form I' the lattice parameters have not been determined, and it must not be ruled out the possibility that this newly detected phase, Form I'', is actually a mixture of phases. However, this goes in contrary to the fact that the low-angle peaks do not belong to the tetragonal or orthorhombic structures, pointing that they must belong to other phases.

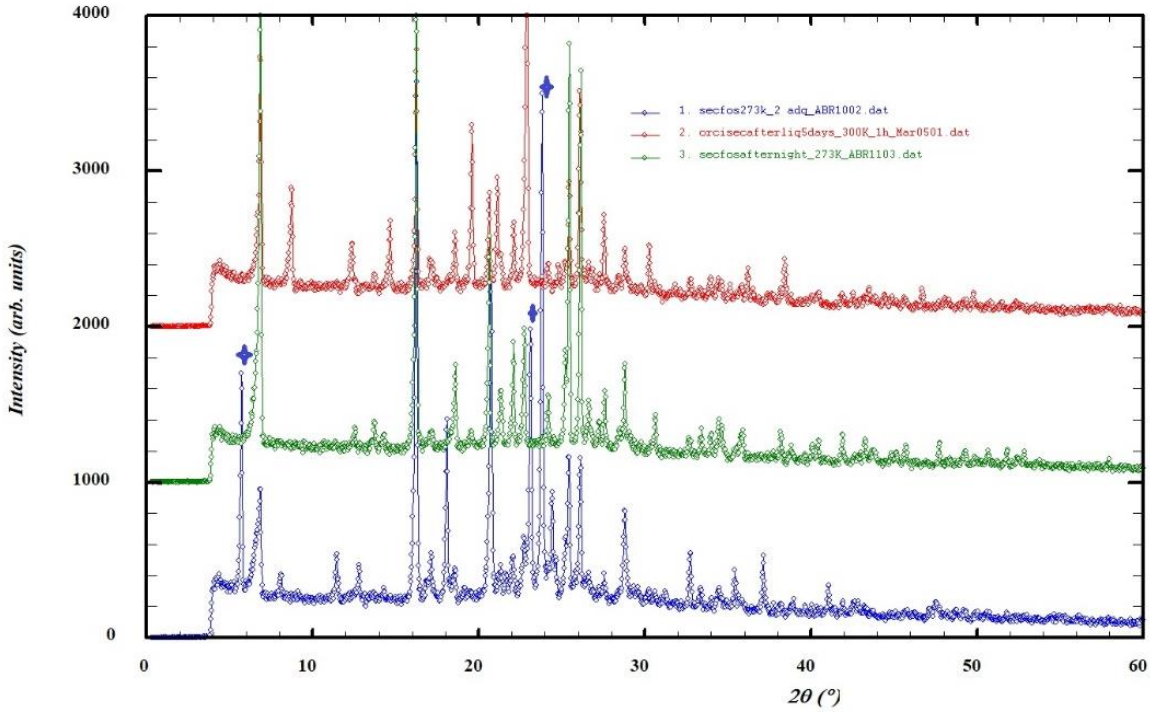

***Figure 4.27**. Experimental spectra at 273 K after a quick cooling of the liquid (blue), evolution of the spectra after 12 hours (green) at the same temperature and the spectra at 300 K obtained from the orthorhombic phase (red)(Form I').*

The heating of the sample obtained after 12 hours shows that the phase is maintained until 360 K, see Figure 4.28. By heating it at 380 K, the spectrum changes, indicating that it transformed. This spectrum corresponds to the spectrum of the tetragonal phase at the same temperature, as shown in Figure 4.28 (although the number of peaks is lower as a consequence of the preferential orientations).

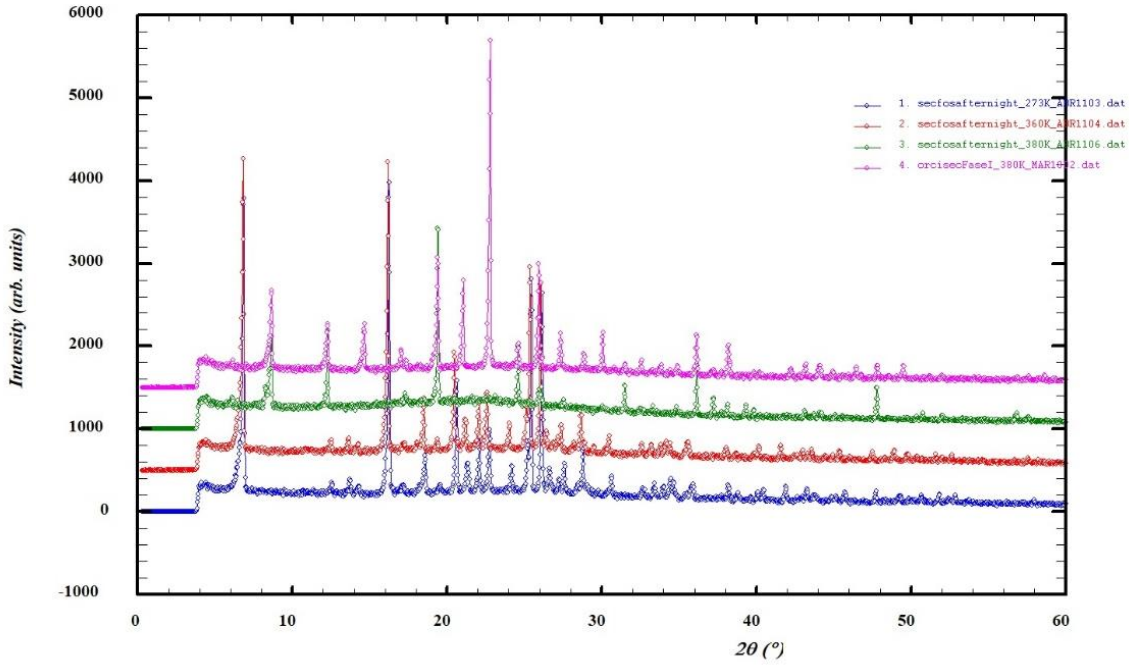

***Figure 4.28**. Heating sequence for polymorph I': 273 K (blue), 360 K (red) and 380 K (green). The spectrum tetragonal form at 380 K (pink) is included in order to show that polymorph I' transformed into the tetragonal phase.*

To summarize, it was concluded that tetragonal form is the stable phase I, being the phase with higher melting point. The unknown Form I' would be the metastable phase and could be related with the highest metastable melting point (at 97 ºC). Form II (orthorhombic) and the unknown Form I'' are more metastable than Form I', but the degree of metastability between the two could not be established. Then, the assignation of the remaining melting point at 84 ºC remains unresolved.

4.6. High pressure DTA

With a high pressure DTA instrument (created by the GMC research group), the behavior of the polymorphs of orcinol was investigated at high pressure. In particular, the objective was to determine the melting temperature of each polymorph at high pressure (while melting enthalpies in these conditions were out of scope). Temperature ranges were in the interval 25 – 140 ºC, while pressure ranged from ambient pressure up to 3 kbar (300 MPa). Setup and sample preparation were explained in Section 3.1.2. In total, seven different samples were prepared and subsequently analyzed. Data was collected both on the heating ramp (with a heating rate of 2 ºC) and on the cooling ramp; however, this latter data was not analyzed (as in the case of DSC, during cooling there can be found out-of-equilibrium states). The instrument, at set time interval (5 s), registered several quantities: sample temperature (both in ºC and V), pressure and voltage difference between sample and reference (in V). Measurements were recorded in .dat files that were analyzed by Excel software. Baseline of every thermogram was found as the interpolation line of the recorded (V, T) values from start right until the onset of the peak. An auxiliary line was drawn as the tangent of the peak in the point where the slope is maximum. Then, the melting temperature was found as the intersection point of the two lines (as shown in Section 3.1.1, Figure 3.3). A visual depiction is given in Figure 4.29. The corresponding pressure at melting point, $P(T_m)$ (which is not equal the pressure set at the start of

the measurement), was determined by considering that, being that the system (the sample) is at constant volume and is made of a pure substance, then, by the phase rule, there is only one independent variable; thus, temperature being set as the free variable, linear interpolations *P(T)* are calculated. By knowing temperature and time at each point it is possible to integrate the peak area (its units are V·s). To transform this result into units of enthalpy it is necessary to know the mass of the sample and perform a calibration analogous in the same way that is done with the DSC. Since the values of enthalpy depend on the pressure the calibration procedure is quite complicated and enthalpy values were not recorded.

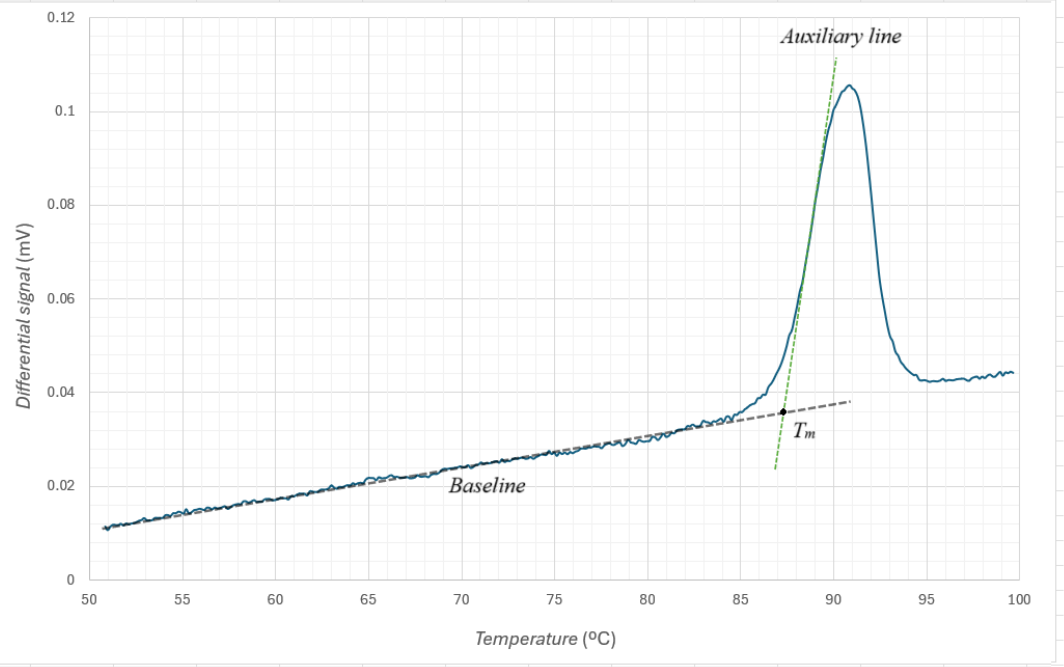

***Figure 4.29**. DTA thermogram with added baseline and auxiliary line utilized to determine melting temperature*

DTA plots of the first heating for different samples, at several pressures, are represented in Figure 4.30. Only the signal corresponding to the melting point has been observed, that increases with pressure.

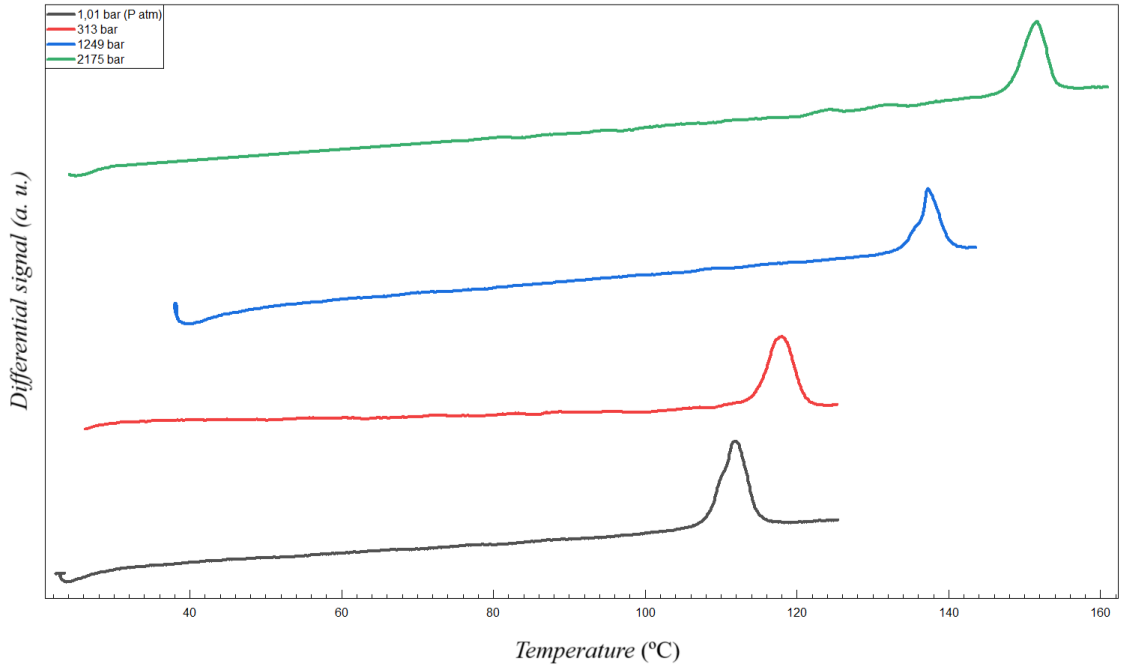

***Figure 4.30**. Comparison of DTA plots of first heating runs of different samples with different pressures at melting point: normal pressure (black), 313 bar (red), 1249 bar (blue) and 2175 bar (green)*

The *T* and *P* values corresponding to the melting for the first heating of the samples have been named I-L in and are represented in Figure 4.31 (blue points). The evolution of the melting temperature with the pressure has been adjusted by means of Eq 4.11.

The first heating runs of the seven samples were always attributed, from the results of DSC, to the stable phase I. By linearly interpolating this data, Eq. 4.11 is found:

$$T[\text{°C}] = (110 \pm 2) + (0{,}013 \pm 0{,}002) \cdot P[\text{bar}] \qquad \text{Eq. 4.11}$$

Or equivalently

$$T[\text{K}] = (384 \pm 2) + (0{,}13 \pm 0{,}02) \cdot P[\text{MPa}] \qquad \text{Eq. 4.12}$$

Notably, melting point of phase I as recorded by DSC is within the error interval of the y-intercept of Eq. 4.11-12.

The same procedure was applied to obtain Eq. 4.13-14 and 4.15-16, representing II-L and III-L boundary lines respectively. For transition II-L (in °C and bar):

$$T[\text{°C}] = (98 \pm 2) + (0{,}018 \pm 0{,}002) \cdot P[\text{bar}] \qquad \text{Eq. 4.13}$$

Or equivalently, in K and MPa:

$$T[\text{K}] = (371 \pm 2) + (0{,}18 \pm 0{,}02) \cdot P[\text{MPa}] \qquad \text{Eq. 4.14}$$

For transition III-L in °C and bar:

$$T[℃] = (82 \pm 2) + (0{,}012 \pm 0{,}002) \cdot P[\text{bar}] \quad \text{Eq. 4.15}$$

Or in K and MPa:

$$T[\text{K}] = (355 \pm 2) + (0{,}12 \pm 0{,}02) \cdot P[\text{MPa}] \quad \text{Eq. 4.16}$$

In Table 4.6 is summarized the data presented in Figure 4.31.

Table 4.6. *Data collected by means of HP-DTA*

I-L		***II-L***		***III-L***		***Non-attributed***	
P (bar)	*T* (℃)	*P* (bar)	*T* (℃)	*P* (bar)	*T* (℃)	*P* (bar)	*T* (℃)
313	114	24	96	144	84	1861	108
611	120	365	105	187	85	2138	112
901	122	533	108	345	87	2256	114
1645	130	704	110	401	86		
1705	135	1031	118	423	86		
2080	137	1048	118	597	87		
2328	139	1124	116	946	91		
		1095	115	1310	97		
		1441	124	1313	97		
		1670	127	1427	100		
		1985	132	1597	99		
		2177	135	1854	106		
		2192	136	1916	107		
				2141	107		

Data was collected to produce an experimental *T(P)* state diagram, fitted in accordance with the results of XRD measurements and DSC at normal pressure, that showed the presence of (at least) three different crystalline structures at normal pressure. The measured data are shown in Table 4.6. and represented in Figure 4.31.

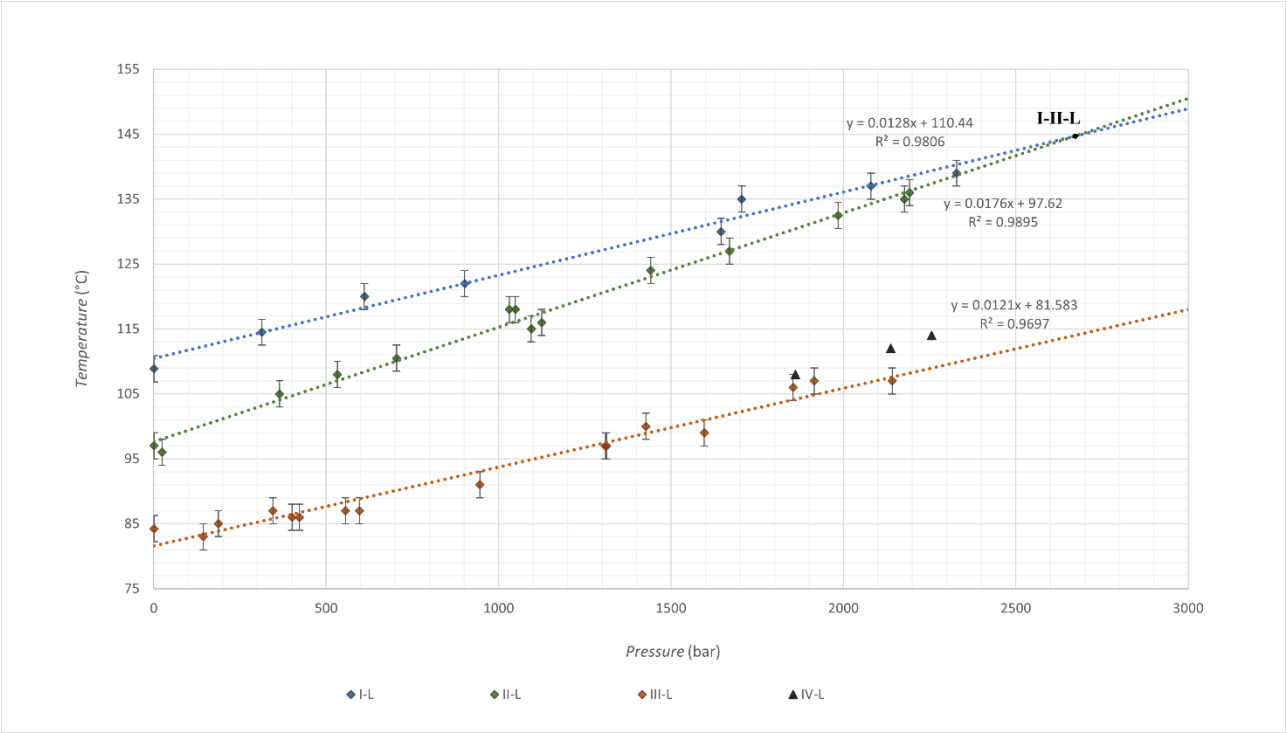

***Figure 4.31**. T(P) experimental plot of measured melting point. Interpolating lines were fitted to draw I-L (blue), II-L (green) and III-L (red) boundary curves. Black triangle marked points could belong to another unknown boundary line*

Interpolated boundary lines I-L and II-L intersect in the upper right portion of the diagram; this is the triple point I-II-L. Utilizing the equations of the interpolation lines permitted to calculate the values of (*P, T*) at the triple point. The values found were:

- $P_{I\text{-}II\text{-}L}$ = 2670 bar (267 MPa)
- $T_{I\text{-}II\text{-}L}$ = 144 ºC (417 K)

In Section 4.3 it was established that, at normal pressure, the relationship between each polymorph is monotropic, but this does not conclude that it holds true for all ranges of pressure. However, considering all possible *T(P)* diagrams as described by Bakhuis-Roozeboom (as in Section 2.4), it's possible to conclude that between phases I and II, at a pressure greater than 267 MPa, the relationship becomes enantiotropic. Meanwhile, the relationship between phases II and III shows overall monotropy.

In the diagram were also reported values (marked by black triangles) that lay above the boundary III-L. Assuming that from XRD results the existence of three metastable phases has been suggested, these points could be attributable to the melting of some of them. However, a more thorough analysis should be conducted at higher pressures to obtain *T(P)* points that could be unequivocally attributed to some boundary line. Alternatively, this could be a new phase appearing at high pressures.

If one were to construct the complete pressure-temperature phase diagram of orcinol, it will be necessary to determine the specific volume of the liquid unequivocally. A simple empirical equation, $V_L = 1{,}1\ V_S$ was proposed by Rietvield *et al.*[60] that was shown to well-approximation for some organic crystals. This relation could be utilized in Clausius-Clapeyron equation to calculate the theoretical slope of boundary phases. From the data collected, only the I-L slope could be calculated as

$$\frac{dP}{dT} = \frac{\Delta H}{T\Delta v} = \frac{162{,}61\ J/g}{383{,}12\ K \cdot 0{,}08826\ cm^3} = 4{,}8091\ \frac{J}{K\ cm^3} = 4{,}8091\ MPa/K \qquad \text{Eq. 4.17}$$

The value found for the slope of I-L phase boundary (expressed as the reciprocate), *dT/dP* = 0,2079 K/MPa, does not seem to be in agreement with experimental data (0,13 K/MPa), hence any further theoretical calculations would probably require a measure of the massic volume of the liquid.

5. Conclusions

In this work, polymorphic forms of orcinol and their thermodynamic relationships were explored. Thermal analyses at normal pressure determined the presence of three different melting points at 108,87 ℃, 97,06 ℃ and 84,24 ℃, attributed to three different solid phases (stable phase I, metastable phase II and supermetastable phase III, respectively) that pure orcinol could assume. It was proposed by thermodynamic arguments that all three phases are monotropically related at normal pressure. XR difractometry was conducted to confirm the attribution of the former melting points to different crystal structures, and to establish the crystal system and lattice parameters of the phases found. From the literature, the existence of two polymorphs is known, with tetragonal and orthorhombic symmetries. XR diffraction allowed to identify the stable phase I with the lattice of tetragonal symmetry. Cooling the sample from the liquid phase gave rise to three different structures, the orthorhombic one (Form II), Form I' and Form I''. Most of the time, the orthorhombic lattice was obtained. In some instances, a newly discovered Form I' appeared from the orthorhombic form, thus indicating that this new phase is more stable. In a single case the sample took another undiscovered structure, Form I'', that later spontaneously evolved into Form I'. Thus, it was concluded that Form I' could be associated with the highest metastable melting point at 97 ºC.The orthorhombic form (Form II) and the unknown Form I'' are more metastable than Form I', but the degree of metastability between both could not be established. Then, the assignation of the remaining phase with melting point at 84 ºC remains unresolved. Moreover, for both Form I' and I'' the respective crystal systems were not determined, because the indexation did not yield uncontestable results. Finally, by means of a high pressure DTA, melting points of orcinol samples were recorded to create an experimental P-T diagram. The data collected was fitted mostly in three different boundary lines, belonging to the transition of each phase to liquid, and they were in agreement with normal pressure DSC data. While at ambient pressure the three phases are monotropically related, it was found that at pressures higher than at the triple point I-II-L (from 267 MPa) the relationship between I and II becomes enantiotropic. Phases II and III are monotropically related overall.

To determine the correct thermodynamic relationship between the two higher metastable structures Form II (orthorhombic) and Form I', more experiments should be conducted. Probably any further analysis would benefit from a synthesis route of metastable forms not left to chance (as is the case with cooling from liquid). Specifically, crystal growth from solution could be employed, as done by Mukherjee *et al*.[51] to obtain the tetrahedral and the orthorhombic form. If Form I'' can be also consistently obtained by a similar procedure, then, to determine the relative stability between Form II and I'', one could repeat the procedure of measuring melting point across all pressure as previously explained. Alternatively, one could utilize FTIR spectroscopy to determine the relative stability of these phases by means of the so-called infrared rule. In fact this rule, proposed by Burger and Ramburger, states that the formation of strong hydrogen bonds is associated with a reduction in entropy and an increase in the frequency of the vibrational modes of those same hydrogen bonds; by that, the polymorph that shows the highest frequency associated with O-H bonds is the most stable. Also, if a single crystal is obtained by solution growth, then the

corresponding XR diffractograms could yield clearer diffractograms that would be more easily indexed, thus determining the actual crystal system and lattice parameters of Form I' and I".

6. Economic analysis of the project

The material resources consist of the equipment used by the Group of Characterization of Materials (GCM) in the Department of Physics at EEBE. To account for expenses related to equipment and licenses, their costs have been calculated based on acquisition cost, estimated lifetime, and usage time during the project (as seen in Tables 9.1 and 9.2). It is assumed that amortization costs are spread evenly over time, as shown in the following formula:

$$Amortization = Acquisition\ cost / (Estimated\ lifetime \times Usage\ time) \quad \text{Eq. 6.1}$$

Thus, it is necessary to determine the useful life of all equipment, as they gradually decrease in value until they become obsolete. Instruments such as the analytical balance, the Tzero press, and the heater are expected to function effectively for 20 years. The DSC and HP-DTA systems are anticipated to have a useful life of about 10 years, primarily due to their resistance to oxidative degradation. The X-ray machine also has an estimated lifespan of 10 years. Computers typically last 5 years, while refrigerators have an expected lifespan between 14 and 17 years. All these costs are illustrated in the relevant tables.

***Table 6.1**. Amortization calculation of fixed costs*

Equipment	**PVP (€)**	**Estimated lifetime (years)**	**Usage time (years)**	**Final cost (€)**
DSC Q100	19700	10	0.09	177.3
HP-DTA	60000	10	0.09	540
X-ray powder diffractometer	220000	10	0.09	1998
Analytical balance	1500	20	0.09	6.75
Refrigerator	136	15.5	0.09	0.79
Heater	28	20	0.09	0.13
Tzero DSC sample encapsulation press	4220	20	0.09	18.99
Computer	899	5	0.09	16.18
Total (€)		**2758.14**		

***Table 6.2**. Calculation of costs of softwares utilized*

Licenses	**Unit Price (€)**	**Estimated lifetime (years)**	**Using time (years)**	**Cost (€)**
Microsoft Office 2019 Standard 32/64 Bit	154.95	5	0.09	21.63
Software control Q100	Free	5	0.09	-
Universal V3.9A TA Instruments	Free	5	0.09	-
Total (€)		**21.63**		

Another consideration is the laboratory materials used throughout the project. Table 6.3 outlines elements with a higher likelihood of breaking or deforming that have been replaced during the project, such as sample pans and lids used in the Tzero Press, as well as the high-pressure capsules for the HP-DTA measurements.

***Table 6.3**. Costs of various spare materials bought*

Spare material	**Unit Price (€)**	**Number of units purchased**	**Cost (€)**
Thermocouple	55.95	2	111.90
Capillary tubes	150	4	600
Tzero DSC pans (per kg of 100)	1.25	46	57.5
Tzero DSC hermetic lids (per kg of 100)	1.3	46	59.8
High pressure capsule (lid capsule, 100 g)	33.9	3	101.7
Total (€)		**930.90**	

Table 6.4 summarizes the gas and transmission pressure liquid expenses incurred during DSC and HP-DTA measurements, contributing to fluid budget control.

***Table 6.4**. Costs of fluid materials*

Fluid material	Unit Price (€)	Number of units purchased	Cost (€)
Nitrogen gas cylinder	80	1	80
Helium gas cylinder	134	1	134
Perfluorinated oil (20 L)	800	0.2	160
Total		**374**	

Sample material (orcinol and orcinol monohydrate) costs are represented in Table 6.5.

***Table 6.5**. Costs of sample materials*

Compound (from Thermo Fischer Scientific)	Amount per pot (g)	Unit Price (€)	Number of pots purchased	Cost (€)
Orcinol 98%	100	508	1	508
Orcinol monohydrate 99%	100	284	1	284
Total (€)		**792**		

Giving an estimated electricity usage of 800 kWh, and based on known provider (Endesa) energy price of 0.1125 €/kWh, this results in an electricity cost of 90 €. Furthermore, accounting for lighting and other electrical usage over the project's duration, the total electricity expense is estimated at around 100 €.

The cost of human resources was calculated on the fact that two people worked on the project, one 200 h and the other 600 h. Estimating an hourly labor cost of 25 €, the total cost for human resources is 20000 €.

Lastly, it is important to account for unforeseen circumstances that may increase project costs. Therefore, an additional contingency of 10% of the total budget has been added to cover such events. The summary of the costs is reported in Table 6.6.

***Table 6.6**. Summary of the costs taken in the project*

Component	**Cost (€)**
Equipment	2758.14
Spare material	930.9
Fuel material	374
Compounds	792
Licences	21.63
Electricity	100
Human resources	20000
Contingency item (10 %)	2497.8
Total cost (€)	27474.47

To conclude, the total cost of the project has been estimated at around 27475 €.

7. Bibliography

1. Pokrovsky, V. Chapter 1: The Concept of Thermodynamic System. 2018, 1–12
2. Gresh, M. T. Thermodynamics. In *Compressor Performance*; Guerin, B., Ed.; Matthew Deans: Pennsylvania, 2018; pp 13–30. https://doi.org/10.1016/B978-0-12-814219-6.00002-7
3. M. J. Moran, H. N. Shapiro, 'Fundamentals of Engineering Thermodynamics', Fourth Edition, Wiley, New York, 2000
4. Rajput, R. K. P-V-T Surfaces and Properties of Ideal Gas. In *Thermal Engineering*; Technology, P. C. of I., Ed.; Laxmi Publications: New Delhi, 2010
5. Huang, K. Some Applications of Thermodynamics. In *Statistical Mechanics*; Technology, I. of, Ed.; Braun-Brumfield, Inc: Massachusetts, 1987; p 31.
6. Galasso, F. S. Chapter 6 – Phase Transitions. In *Structure, Properties and Preparation of Perovskite-Type Compounds*; Pregamon Press: Oxford, 1969; pp 115–121. https://doi.org/10.1016/B978-0-08-012744-6.50009-4
7. Hernández Clusa, C. Determinación de Diagramas de Equilibrio Presión-Temperatura En Compuestos Orgánicos. *Proy. Final Grado* 2014, 1–90.
8. Ferreira, A. G. M.; Lobo, L. Q. The Low-Pressure Phase Diagram of Sulfur. *J. Chem. Thermodyn.* 2011, *43* (2), 95–104. https://doi.org/10.1016/j.jct.2010.07.007
9. R. E. Sonntag, C. Borgnakke, and G. J. Van Wylen, 'Fundamentals of Thermodynamics', Sixth Edition, Wiley, Singapore, 2003.
10. Fermi, E., 'Thermodynamics'. Courier Corporation, 2012.
11. Boltzmann, L., 'Lectures on Gas Theory', University of California Press eBooks, 1964. https://doi.org/10.1525/9780520327474
12. Escuer, J. H. Determinació Del Diagrama Pressió-Temperatura Dels Materials Moleculars. Grau en Eng. Química 2016
13. Stishov, S. M. Introduction. In *Phase Transitions for beginners*; World Scientific Publishing Co. Pte. Ltd: Russia, 2018; pp 1–7. https://doi.org/10.1515/9783110289039.545.
14. Chistyakov, D.; Sergeev, G. The Polymorphism of Drugs: New Approaches to the Synthesis of Nanostructured Polymorphs. *Pharmaceutics,* 2020, *12* (1), 1–9. https://doi.org/10.3390/pharmaceutics12010034
15. Barrio, M., Huguet, J., Robert, B., Rietveld, I., Céolin, R., & Tamarit, J. (2017). Pressure-temperature phase diagram of the dimorphism of the anti-inflammatory drug nimesulide. *International Journal of Pharmaceutics*, 525(1), 54–59. https://doi.org/10.1016/j.ijpharm.2017.04.016
16. Chen, B., Liu, X., Wang, Y., Bai, J., Liu, X., Xiang, G., Liu, W., Zhu, X., Cheng, J., Lu, L., Zhang, G., Zhang, G., Dai, Z., Zi, S., Yang, S., & Jiang, H. (2023). Production of the antidepressant orcinol glucoside in Yarrowia lipolytica with yields over 6,400-fold higher than plant extraction. *PLoS Biology*, 21(6), e3002131. https://doi.org/10.1371/journal.pbio.3002131
17. Li, J., He, P., Zhang, J., & Li, N. (2021). Orcinol glucoside improves the depressive-like behaviors of perimenopausal depression mice through modulating activity of hypothalamic–pituitary–adrenal/ovary axis and activating BDNF- TrkB-CREB signaling pathway. *Phytotherapy Research*, 35(10), 5795–5807. https://doi.org/10.1002/ptr.7237
18. Lian, C., Gong, W., Zhao, X., Sun, P., Hu, S., Zhou, G., Zhang, Q., & Qin, L. (2024). Orcinol gentiobioside inhibits RANKL-induced osteoclastogenesis by promoting apoptosis and suppressing autophagy via the JNK1 signaling. *Journal of Ethnopharmacology*, 328, 118060. https://doi.org/10.1016/j.jep.2024.118060

19. Lee, E. H. A Practical Guide to Pharmaceutical Polymorph Screening & Selection. *Asian J. Pharm. Sci.* 2014, *9* (4), 163–175. https://doi.org/10.1016/j.ajps.2014.05.002
20. Hadjittofis, E., Isbell, M. A., Karde, V., Varghese, S., Ghoroi, C., & Heng, J. Y. Y. (2018). Influences of crystal anisotropy in pharmaceutical process development. *Pharmaceutical Research*, 35(5). https://doi.org/10.1007/s11095-018-2374-9
21. Gadamasetti, K. G.; 'Process Chemistry in the Pharmaceutical Industry', 1st ed.; Press, C., Ed.; Headquarters Marcel Dekker: New Brunswick, 1999.
22. Kelton, K.; Greer, A. Chapter 1-Introduction. In *Nucleation in Condensed Matter: Applications in Materials and Biology*; 2020 Elsevier Ltd.: Oxford, 2010; Vol. 15, pp 1–15. https://doi.org/10.1016/S1470-1804(09)01501-6.
23. Sharma, A.; Mishra, R.; Poonam, T. Polymorphism in Pharmaceutical Compounds. Adv. Futur. Trends Mater. Sci. 2011, No. January, 39–47.
24. Vrani, E. Recent Advances in the Identification and Prediction of Polymorphs. 2003, 3 (2), 32–36. https://doi.org/https://doi.org/10.17305/bjbms.2003.3525
25. Hadjittofis, E., Isbell, M. A., Karde, V., Varghese, S., Ghoroi, C., & Heng, J. Y. Y. (2018). Influences of crystal anisotropy in pharmaceutical process development. *Pharmaceutical Research*, 35(5). https://doi.org/10.1007/s11095-018-2374-9
26. Rodríguez-Spong, B.; Price, C. P.; Jayasankar, A.; Matzger, A. J.; Rodríguez-Hornedo, N. General Principles of Pharmaceutical Solid Polymorphism: A Supramolecular Perspective. *Adv. Drug Deliv. Rev.* 2004, *56* (3), 241–274. https://doi.org/10.1016/j.addr.2003.10.005.
27. Bernstein, J.; 'Polymorphism in Molecular Crystals'. Second edition. Oxford: Oxford University Press, 2020.
28. Haleblian, J.; McCrone, W. Pharmaceutical Applications of Polymorphism. *J. Pharm. Sci.* 1969, *58* (8), 911–929. https://doi.org/10.1002/jps.2600580802.
29. Rietveld, I. B. Phase Equilibria and Their Applications. *Eur. Phys. J. Spec. Top.* 2017, *226* (5), 817–822. https://doi.org/10.1140/epjst/e2016-60377-2.
30. Rietveld, I. B.; Céolin, R.; Tamarit, J. Polymorphism and Isopolymorphism. *Press* 1999, 1–36.
31. Kadam, K. P.; Chavan, R. P. Evaluation of Various Polymorphs by Different Techniques and Their Characterization A Review. *J. Eng. Sci.* 2016, *5* (6), 29–34.
32. Menczel, J. D., Andre, R., Kohl, W. S., Krongauz, V. V., Lőrinczy, D., Reading, M., & Grebowicz, J. (2023). 'Fundamentals of DSC'. In Elsevier eBooks (pp. 1–189). https://doi.org/10.1016/b978-0-12-811347-9.00005-9
33. Akash, M.S.H., Rehman, K. (2020). Differential Scanning Calorimetry. In 'Essentials of Pharmaceutical Analysis'. Springer, Singapore. https://doi.org/10.1007/978-981-15-1547-7_17
34. Singh, N.; Investigation on transport properties and structural characterization of some nanomaterials for fabrication of hybrid supercapacitors, 2014, https://doi.org/10.13140/RG.2.1.2345.2245
35. LG.W.H. Höhne; H.K. Cammenga; W. Eysel; E. Gmelin; W. Hemminger. The Temperature Calibration of Scanning Calorimeters. *Thermochim. Acta,* 1990, *160* (1), 1–12. https://doi.org/https://doi.org/10.1016/0040-6031(90)80235-Q
36. Shandilya, D.; Sharma, S. Applications of Thermoanalytical Techniques for Studying Polymorphism and Solid-State Transformations in Pharmaceutical Industry. *Anal. Chem. an Indian J. ACAIJ* **2012**, *11* (7,8), 249–259. https://doi.org/0974-7419. 249-259
37. Mukasyan, A. S.; DTA/TGA-Based Methods. *Concise Encyclopedia of Self-Propagating High-Temperature Synthesis*. United States: Elsevier Inc, 2017. 93–95.
38. https://www.hitachi-hightech.com/global/en/knowledge/analytical-systems/thermal-analysis/basics/dta.html URL consulted on 01/10/2024
39. Würflinger, A. (1975). Differential thermal analysis under high pressure IV: Low-temperature DTA of solid-solid and solid-liquid transitions of several hydrocarbons up to 3 kbar. *Berichte Der Bunsengesellschaft Für Physikalische Chemie*, *79*(12), 11951201. https://doi.org/10.1002/bbpc.19750791206

40. Li, P., Teng, L., Guo, M., Zhang, M., & Seetharaman, S. (2011b). Oxidation kinetics of ALN under CO2 atmosphere. *Metallurgical and Materials Transactions B*, 43(2), 406–412. https://doi.org/10.1007/s11663-011-9611-5
41. Saadatkhah, N. *et al*.; Experimental Methods in Chemical Engineering: Thermogravimetric Analysis—TGA. *Canadian journal of chemical engineering* 98.1 (2020): 34–43.
42. Kohli, R. *Methods for Monitoring and Measuring Cleanliness of Surfaces*, 1st ed.; Gifford, C., Ed.; Elsevier: Amsterdam, 2012; Vol. 4. https://doi.org/10.1016/B978-1-4377-7883-0.00003-1
43. Cantor, B.; 'Bragg's Law.' The Equations of Materials. Oxford: Oxford University Press, 2020.
44. Thomas, E. L.; Millican, J. N.; Okudzeto, E. K.; Chan, J. Y. Crystal Growth and the Search for Highly Correlated Intermetallics. *Comments Inorg. Chem.* 2006, *27* (1–2), 1–39. https://doi.org/10.1080/02603590600666215
45. Law, D.; Zhou, D. Solid-State Characterization and Techniques. In *Developing Solid Oral Dosage Forms: Pharmaceutical Theory and Practice: Second Edition*; Elsevier Inc., 2017; pp 59–84. https://doi.org/10.1016/B978-0-12-802447-8.00003-0
46. Céolin R, Rietveld I. B. (2016). X-ray crystallography, an essential tool for the determination of thermodynamic relationships between crystalline polymorphs. *Ann Pharm* Fr 74:12-20.
47. Doğan, F., Özdek, N., Selçuki, N. A., & Kaya, İ. (2019). The synthesis, characterization and effect of molar mass distribution on solid-state degradation kinetics of oligo(orcinol). *Journal of Thermal Analysis and Calorimetry*, 138(1), 163–173. https://doi.org/10.1007/s10973-019-08211-x
48. Wang, L., Cheng, Z., Djouonkep, L.D.W. *et al.*; Synthesis and Properties of Biodegradable Polyesters Based on Orcinol. *J Polym Environ* 31, 4314–4325 (2023). https://doi.org/10.1007/s10924-023-02887-x
49. Tothadi, S., Mukherjee, A., & Desiraju, G. R. (2011). Shape and size mimicry in the design of ternary molecular solids: towards a robust strategy for crystal engineering. *Chemical Communications*, 47(44), 12080. https://doi.org/10.1039/c1cc14567c
50. Kubendiran, B., Pramanik, G., Kumar, M., De, P. K., & Kole, G. K. (2022). Mechanochemical synthesis and structure analysis of binary cocrystals of extended bis-pyridyl spacers with resorcinol and orcinol. Journal of Molecular Structure, 1274, 134470. https://doi.org/10.1016/j.molstruc.2022.134470
51. A.Mukherjee, P.Grobelny, T.S.Thakur, G.R.Desiraju, *Crystal Growth and Design*, 2011, 11, 2637, DOI: 10.1021/cg200361x
52. Tothadi, S., & Desiraju, G. R. (2012). Unusual co-crystal of isonicotinamide: the structural landscape in crystal engineering. *Philosophical Transactions of the Royal Society a Mathematical Physical and Engineering Sciences*, 370(1969), 2900–2915. https://doi.org/10.1098/rsta.2011.0309
53. Mozaffari, P., Järvik, O., & Baird, Z. S. (2020). Vapor pressures of phenolic compounds found in pyrolysis oil. Journal of Chemical & Engineering Data, 65(11), 5559–5566. https://doi.org/10.1021/acs.jced.0c00675
54. Kirithivasan, M. (2022). Application of amorphous classification system and glass forming ability in pre-formulation design of small organic molecules. https://odr.chalmers.se/items/60cc7cf0-1ae2-47bb-9a79-0d21abd0dee8
55. Safari, F., Olejniczak, A., & Katrusiak, A. (2020). Pressure-Promoted solvation of resorcinol. *Crystal Growth & Design,* 20(5), 3112–3118. https://doi.org/10.1021/acs.cgd.9b01732
56. Reported in the specification sheet of the product at the website https://www.thermofisher.com/order/catalog/product/129550250 (consulted on 04/10/2024)
57. A.Mukherjee, P.Grobelny, T.S.Thakur, G.R.Desiraju CCDC 818142: Experimental Crystal Structure Determination, 2011, DOI: 10.5517/ccwgbrd
58. A.Mukherjee, P.Grobelny, T.S.Thakur, G.R.Desiraju CCDC 818143: Experimental Crystal Structure Determination, 2011, DOI: 10.5517/ccwgbrd
59. Rodriguez-Carvajal J., Roisnel T., Gonzales-Platas J. (2005). Full-Prof suite version 2005. Laboratoire Léon Brillouin, CEA-CNRS, CEN Saclay, France

60. Rietveld, I. B., Negrier, P., Barrio, M., Allouchi, H., Ceolin, R., & Tamarit, J. (2020). Crystalline tetrazepam as a case study on the volume change on melting of molecular organic compounds. *International Journal of Pharmaceutics*, 593, 120124. https://doi.org/10.1016/j.ijpharm.2020.120124